

Review

# High Energy Radiation from Spider Pulsars

Chung Yue Hui <sup>1,\*</sup>  and Kwan Lok Li <sup>2</sup>

<sup>1</sup> Department of Astronomy and Space Science, Chungnam National University, Daejeon 34134, Korea

<sup>2</sup> Institute of Astronomy, National Tsing Hua University, Hsinchu 30013, Taiwan; lilirayhk@gmail.com

\* Correspondence: huichungyue@gmail.com

Received: 30 June 2019; Accepted: 4 December 2019; Published: 13 December 2019



**Abstract:** The population of millisecond pulsars (MSPs) has been expanded considerably in the last decade. Not only is their number increasing, but also various classes of them have been revealed. Among different classes of MSPs, the behaviours of black widows and redbacks are particularly interesting. These systems consist of an MSP and a low-mass companion star in compact binaries with an orbital period of less than a day. In this article, we give an overview of the high energy nature of these two classes of MSPs. Updated catalogues of black widows and redbacks are presented and their X-ray/ $\gamma$ -ray properties are reviewed. Besides the overview, using the most updated eight-year Fermi Large Area Telescope point source catalog, we have compared the  $\gamma$ -ray properties of these two MSP classes. The results suggest that the X-rays and  $\gamma$ -rays observed from these MSPs originate from different mechanisms. Lastly, we will also mention the future prospects of studying these spider pulsars with the novel methodologies as well as upcoming observing facilities.

**Keywords:** pulsars; neutron stars; binaries; X-ray;  $\gamma$ -ray

## 1. What Are Millisecond Pulsars?

Rotation-powered pulsars, which act as unipolar inductors by coupling the strong magnetic field and fast rotation, radiate at the expense of their rotational energy. As a result, the rotation of a pulsar gradually slows down as it ages. When the rotation becomes too slow to sustain the particles' acceleration in their magnetospheres, the radiation beam shuts down. In such a case, we say a pulsar is “dead”. While their magnetospheric particle accelerators have been turned off, other emission mechanisms (e.g., accretion) can still possibly work in these dead pulsars.

By the time of writing, there are 2702 pulsars in total, including radio pulsars, radio-quiet  $\gamma$ -ray pulsars and magnetars [1]. In Figure 1, we show the distribution of their period  $P$  and period derivative  $\dot{P}$ . Applying a clustering analysis in this 2D parameter space with  $k$ -means partitioning, the whole population can be divided into two parts. The largest one is displayed as black dots in Figure 1. This partition spans a range of  $P \sim 0.02 - 23.5$  s and  $\dot{P} \sim 5 \times 10^{-18} - 5 \times 10^{-10}$  s/s. This group includes canonical pulsars as well as magnetars. Assuming the surface magnetic field is dipolar and the rotational energy of the pulsar goes entirely to the dipolar radiation, one is able to estimate their surface magnetic field strength  $B_s$  and their characteristic age  $\tau$  as:

$$B_s \simeq \sqrt{\frac{3c^3 I}{2\pi^2 R^6} P \dot{P}} \sim 3 \times 10^{19} \sqrt{P \dot{P}} \text{ G} \quad (1)$$

and

$$\tau = \frac{P}{2\dot{P}} \quad (2)$$

where the radius  $R$  and the moment of inertia  $I$  of the neutron star are taken to be  $10^6$  cm and  $10^{45}$  g cm<sup>2</sup> respectively.

These imply that the surface field strength and the characteristic age of this group are at the order of  $B_s \sim 10^{10} - 10^{15}$  G and  $\tau \sim 10^3 - 10^8$  years (see Figure 1). As a canonical pulsar ages and spins down, it moves toward the lower right in the  $P - \dot{P}$  diagram. One should note that there is an absence of systems at the lower right region in the diagram. Such a region is a so-called “graveyard” zone. The dashed line on Figure 1 is known as the death line and separates the neutron stars that can sustain particle acceleration in their inner magnetospheres from those that cannot [2]. On the other hand, there is a dispersed group at the upper right region of the  $P - \dot{P}$  diagram. These objects with surface dipolar fields  $> 10^{14}$  G are magnetars.

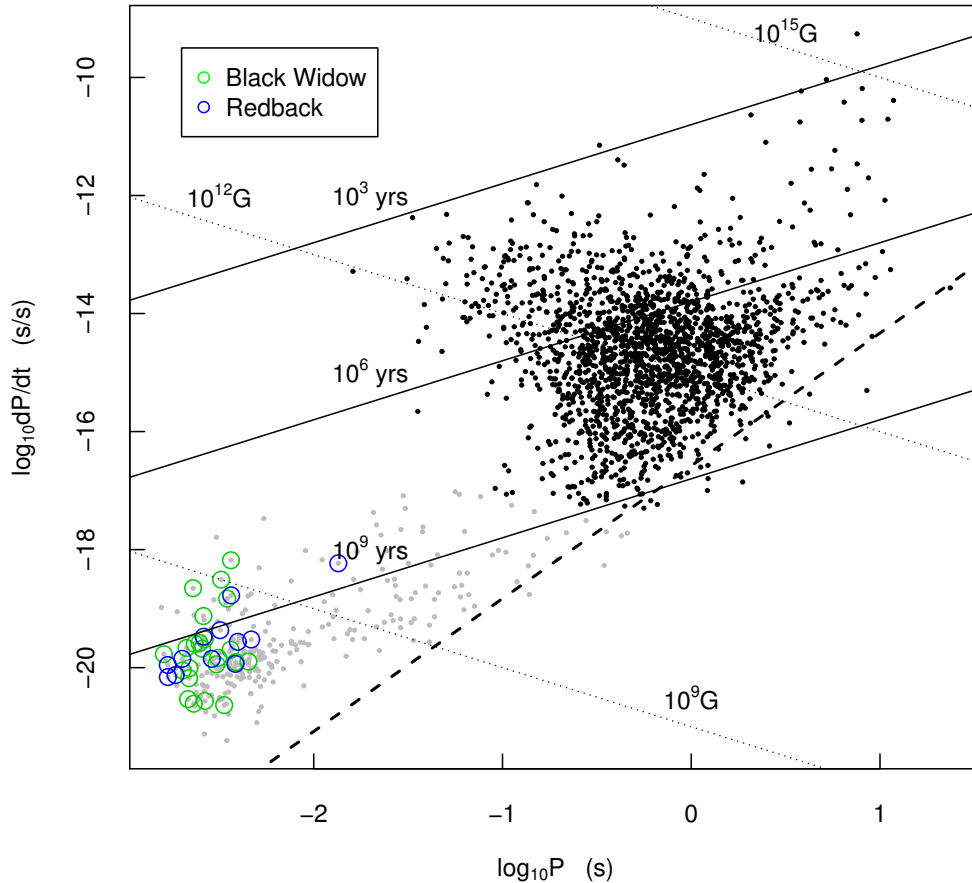


**Figure 1.** Period–period derivative ( $P-\dot{P}$ ) diagram of all currently known pulsars. The population can be divided into two groups (black and grey dots) based on  $k$ -means partitioning. The locations of black widow and redback millisecond pulsars (MSPs) in this parameter space are highlighted by the green and blue circles, respectively. Lines of constant dipolar surface magnetic field (Equation (1)) and characteristic age (Equation (2)) are shown. The dashed line illustrates the death line for radio pulsars by assuming a multipolar magnetic field configuration [2].

The other partition is clustered at the lower left corner of the  $P - \dot{P}$  diagram, which spans a range of  $P \sim 0.001 - 0.5$  s and  $\dot{P} \sim 5 \times 10^{-22} - 10^{-17}$  s/s. The spin parameters imply these pulsars have a weak magnetic field at the surface  $B_s \sim 10^7 - 10^{11}$  G and as old as  $\tau \sim 10^9 - 10^{10}$  years. These are commonly referred to as millisecond pulsars (MSPs). They are displayed as the grey dots in Figure 1.

It is a consensus that MSPs originate from evolved compact binaries. The standard scenario for the formation of MSP is that a dead pulsar is rejuvenated through accreting material from its binary companion [3]. During this “recycling” phase, the system appears as a low-mass X-ray binary (LMXB). While the details of the magnetic field decay is still a subject under discussion (e.g., [4]), the surface field of the neutron star can be somehow buried by the accretion. Approaching the end of this phase (on a Gyr timescale), the neutron star will gain sufficient angular momentum and resuscitate particle

acceleration in the magnetosphere and hence the pulsed radiation again. This marks the birth of a rotation-powered MSP. This scenario was proposed shortly after the discovery of the first MSP PSR B1937+21 [5]. The fast rotations, weak surface magnetic fields and old ages of MSPs are all found to be consistent with this recycling scenario [3].

## 2. Fermi Gamma-Ray Space Telescope—A Game Changer

Since the discovery of the first pulsar in 1967 [6], radio observations have been the major drive for the progress in pulsar astronomy for a long time. For hunting pulsars, a number of extensive radio surveys have been carried out. For example, Parkes multibeam pulsar survey discovered  $\sim 800$  pulsars in 1997–2004 ([7–9]). Once the sky positions of pulsars have been pin-pointed by the radio telescopes, multiwavelength investigations of their nature can be carried out. However, a survey of pulsars simply based on radio observations has certain limitations. For example, the ground-based radio observatories cannot provide a full sky coverage and a high cadence monitoring of their behaviour.

The field of pulsar survey has been changed since 2008 after the Fermi gamma-ray space telescope was launched. The major detector carried by Fermi is the large area telescope (LAT) which has several major improvements in its instrumental performance in comparison with its predecessors (e.g., EGRET) (see [10] for a recent review). While the positional error attained by EGRET was at the order of a few degrees, LAT has improved this by reducing the error to the order of arcminute. This is particularly important for multi-wavelength follow-up investigations (see below). Moreover, the effective area of LAT is  $\sim 7000\text{--}8000\text{ cm}^2$  in 1–100 GeV, which is more than five times larger and covers a much wider energy range than its predecessors. Furthermore, the large field of view of LAT ( $>2$  steradian), which is more than four times larger than that of EGRET, enables it to perform a survey of the whole sky every  $\sim 3$  h. This provides a much more complete sky coverage than any radio pulsar survey. Moreover, it enables a high cadence monitoring of the  $\gamma$ -ray sources almost without interruption. This turns out to be very important for studying a special class of MSPs (see Section 4).

All the data acquired by LAT are accumulated and this enables us to detect fainter sources. 5065 sources have been detected with significance  $> 4\sigma$  by using eight years LAT data [11]. The natures of more than one-fourth of these  $\gamma$ -ray sources remain unknown. These unidentified Fermi objects provide a large discovery space for hunting new MSPs (e.g., [12]). By imposing a set of selection criteria on these unidentified  $\gamma$ -ray sources, MSP-like candidates can be selected for multiwavelength identifications. In our previous work [12], we adopted the following selection criteria: (1) High galactic latitude, (2) absence of long-term  $\gamma$ -ray variability and (3) spectral shape similar to those of pulsars (i.e., a power-law with an exponential cut-off at a few GeV). Condition 1 was imposed as MSPs are old objects and should be located far away from their birth places (i.e., Galactic plane). Condition 2 is imposed for discriminating them from the active galactic nuclei (AGNs).

Since the discovery of pulsar [6], radio all-sky surveys have played a major role in advancing the pulsar astronomy (e.g., [9]). However, a lot of telescope time can be wasted on the blank regions in such blind surveys. On the other hand, the locations of the  $\gamma$ -ray sources uncovered by Fermi essentially provide us with a “treasure map” for hunting pulsars. Once the MSP-like candidates have been identified, efforts can be devoted to these sources in searching multiwavelength counterparts within their  $\gamma$ -ray positional error ellipses and identifying their nature. As we have mentioned, the much-improved accuracy of positional determination by LAT can significantly reduce the number of sources in the field from entering the  $\gamma$ -ray error ellipses by chance. This strategy has been found to be rather efficient at discovering new MSPs. Some sources have modulations found in X-ray and optical regimes with periodicities shorter than a day. This is similar to the orbital modulations that have been seen in MSPs (see Sections 3 and 4). Such property makes these sources the promising MSP candidates.

The discovery of PSR J2339-0533 provides an example to illustrate the synergy of multiwavelength investigations of unidentified  $\gamma$ -ray sources. A bright  $\gamma$ -ray source 0FGL J2339.8-0530 was firstly discovered in the first three months of data collected by Fermi LAT [13]. Within its  $\gamma$ -ray positional error

ellipse, a bright X-ray source CXOU J233938.7-053305 was identified as the X-ray counterpart [14,15]. From the better constrained X-ray position, the optical counterpart has also been found [14,15]. Interestingly, modulations with a period of  $\sim 4.6$  h were discovered in both X-ray and optical regimes [14,15]. These properties are remarkably similar to those that have been observed in some MSP binaries which could originate from the interaction between the pulsar wind and the ablated material from its companion and the heating of the stellar surface of the companion by wind collision. Subsequently, a rotational period of 2.8 ms was detected in radio by the Green Bank Telescope [16].

Among different types of MSPs, the behaviour of a group of so-called spider MSPs are the most interesting. Spider MSPs can be divided into two classes—black widows and redbacks. From the distribution of minimum companion mass and the orbital period of binary MSPs in the galactic field (see Figure 1 in [17]), these two classes are obviously distinct from the other systems. In Tables 1 and 2, we compiled the updated catalogues of all known spider MSPs in the galactic field and globular clusters, separately. Currently, there are 44 confirmed black widows systems that have been detected with 27 in the galactic field and 17 reside in globular clusters. For redbacks, there are 26 in total with 14 systems confirmed in the the galactic field and 12 in globular clusters. The distributions of black widows and redbacks in the  $P - \dot{P}$  diagram are illustrated in Figure 1. In Figure 2, we show their spatial distribution in our galaxy. In the last decade, there have been many interesting high energy phenomena that have been observed from these spider pulsars. These systems contain low-mass companion stars in tight orbits. The interactions between the MSPs and their companions results in many interesting high energy phenomena. In the following sections, we will give an overview of their emission properties in X-ray and  $\gamma$ -ray.

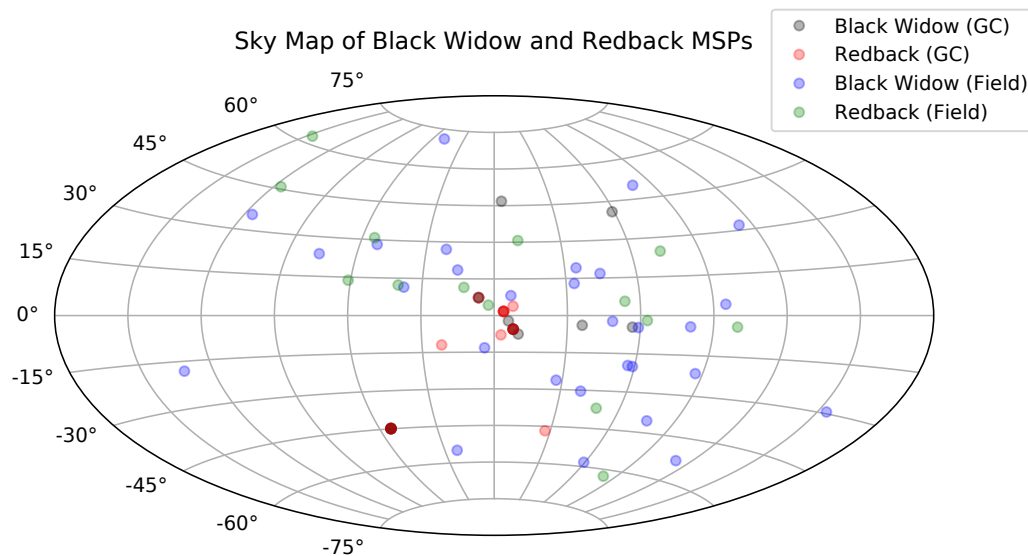


**Figure 2.** Galactic distributions of confirmed spider pulsars. The dark red points are the results of overlapping of redbacks and black widows in the same globular cluster.

**Table 1.** Properties of black widows (BW-F) and redbacks (RB-F) in the galactic field.

Name	Type	Spin Period (ms)	Optical	X-Ray	Gamma-Ray	Modulation <sup>(1)</sup>	Pulsations <sup>(2)</sup>	References
J0023+0923	BW-F	3.05	Y	Y	Y	O	RG	[18–20]
J0251+2606	BW-F	3.86			Y	O	RG	[21,22]
J0610-2100	BW-F	3.86	Y		Y	o	RG	[23,24]
J0952-0607	BW-F	1.41	Y	Y	Y	O	RG	[22,25,26]
J1023+0038	RB-F	1.69	Y	Y	Y	OXg	RGXO	[27–32]
J1048+2339	RB-F	4.67	Y	Y	Y	OX	RG	[21,33,34]
J1124-3653	BW-F	2.41		Y	Y	Ox	RG	[22,35,36]
J1227-4853	RB-F	1.69	Y	Y	Y	Og	RGX	[20,37–40]
J1301+0833	BW-F	1.84	Y		Y	O	RG	[41,42]
J1302-3258	RB-F	3.77			Y		RG	[35]
J1311-3430	BW-F	2.56	Y	Y	Y	Og	RG	[20,43–45]
J1431-4715	RB-F	2.01	Y		Y	O	RG	[46,47]
J1446-4701	BW-F	2.19		Y	Y		RG	[20,48]
J1513-2550	BW-F	2.12			Y		RG	[49]
J1544+4937	BW-F	2.16	Y		Y	O	RG	[50,51]
J1555-2908	BW-F	1.79			Y		RG	[52]
J1622-0315	RB-F	3.85	Y		Y	O	RG	[49]
J1628-3205	RB-F	3.21	Y	Y	Y	O	RG	[20,41,42]
J1641+8049	BW-F	2.02	Y		Y		RG	[53]
J1723-2837	RB-F	1.86	Y	Y		oX	R	[54,55]
J1731-1847	BW-F	2.34		Y	Y		R	[20,48]
J1745+1017	BW-F	2.65			Y		RG	[56]
J1805+0615	BW-F	2.13			Y		RG	[21]
J1810+1744	BW-F	1.66	Y	Y	Y	O	RG	[19,20,35]
J1816+4510	RB-F	3.19	Y	Y	Y	o	RG	[20,57,58]
J1832-38	BW-F	1.87			Y		R	[52]
J1908+2105	RB-F	2.56	Y		Y		RG	[21,47]
J1928+1245	BW-F	3.02	Y				R	[59]
J1957+2516	RB-F	3.96	Y				R	[47,60]
J1959+2048	BW-F	1.61	Y	Y	Y	OXg	RG	[61–64]
J2017-1614	BW-F	2.31	Y		Y	o	RG	[49]
J2047+1053	BW-F	4.29		Y	Y		RG	[20,41]
J2051-0827	BW-F	4.51	Y	Y	Y	O	RG	[20,65,66]
J2052+1218	BW-F	1.99			Y	O	RG	[21,22]
J2055+3829	BW-F	2.09					R	[67]
J2115+5448	BW-F	2.60			Y		RG	[49]
J2129-0429	RB-F	7.62	Y	Y	Y	OX	RG	[35,68,69]
J2214+3000	BW-F	3.12	Y	Y	Y	O	RG	[18,20,70]
J2215+5135	RB-F	2.61	Y	Y	Y	oX	RG	[19,35,36]
J2234+0944	BW-F	3.63			Y		RG	[18]
J2241-5236	BW-F	2.19		Y	Y	Og	RG	[20,22,71,72]
J2256-1024	BW-F	2.29	Y	Y	Y	OX	RG	[19,35,36]
J2339-0533	RB-F	2.88	Y	Y	Y	OX	RG	[14,73]

<sup>(1)</sup> O = Significant optical orbital modulation; o = possible optical orbital modulation; X = significant X-ray orbital modulation; x = possible X-ray orbital modulation; g = possible gamma-ray orbital modulation. <sup>(2)</sup> R = radio pulsations; G = gamma-ray pulsations; X = X-ray pulsations; O = optical pulsations.

**Table 2.** Properties of black widows (BW-GC) and redbacks (RB-GC) in the globular clusters.

Name	Type	Spin Period (ms)	Optical	X-Ray	Gamma-Ray	Modulation <sup>(1)</sup>	Pulsations <sup>(2)</sup>	References
J0024-7204I	BW-GC	3.48		Y			R	[74,75]
J0024-7204J	BW-GC	2.10		Y			R	[74,75]
J0024-7204O	BW-GC	2.64		Y			R	[74,75]
J0024-7204P	BW-GC	3.64					R	[74]
J0024-7204R	BW-GC	3.48		Y			R	[74,75]
J0024-7204V	RB-GC	4.81					R	[74]
J0024-7204W	RB-GC	2.35	Y	Y		oX	R	[74,76,77]
J1518+0204C	BW-GC	2.48	Y			o	R	[78]
J1641+3627E	BW-GC	2.49					R	[79]
J1701-3006B	RB-GC	3.59	Y	Y		O	R	[75,80,81]
J1701-3006E	BW-GC	3.23					R	[80]
J1701-3006F	BW-GC	2.29					R	[80]
J1740-5340	RB-GC	3.65	Y	Y		Ox	R	[75,82,83]
J1748-2021D	RB-GC	13.50					R	[84]
J1748-2446A	RB-GC	11.56					R	[85]
J1748-2446O	BW-GC	1.68					R	[86]
J1748-2446P	RB-GC	1.73					R	[86]
J1748-2446ad	RB-GC	1.40					R	[87]
J1807-2459A	BW-GC	3.06					R	[80]
J1823-3021F	RB-GC	4.85					R	[80]
J1824-2452G	BW-GC	5.91		Y		x	R	[75,88]
J1824-2452H	RB-GC	4.63	Y	Y		Ox	R	[75,88,89]
J1824-2452I	RB-GC	3.93	Y	Y			RX	[88,90,91]
J1824-2452J	BW-GC	4.04					R	[88]
J1824-2452L	BW-GC	4.10					R	[88]
J1836-2354A	BW-GC	3.35					R	[92]
J1911+0102A	BW-GC	3.62					R	[93]
J1953+1846A	BW-GC	4.89	Y	Y		O	R	[75,79,94]
J2140-2310A	RB-GC	11.02					R	[95]

<sup>(1)</sup> O = Significant optical orbital modulation; o = possible optical orbital modulation; X = significant X-ray orbital modulation; x = possible X-ray orbital modulation; g = possible gamma-ray orbital modulation. <sup>(2)</sup> R = radio pulsations; G = gamma-ray pulsations; X = X-ray pulsations; O = optical pulsations

### 3. Black Widows

While the recycling scenario has been proposed for more than 30 yrs, many details of the formation process of MSPs remain uncertain. As mentioned before, an MSP is expected to be the end product of the evolution of a compact binary. One may be puzzled to notice that ~30% of the known MSPs in the galactic field are found to be isolated [96]. One proposed possibility to explain their solitude is that the high energy emission from these rejuvenated pulsars have ablated their companions [97]; and the companion stars will eventually evaporate entirely.

This proposed scenario was motivated by the discovery of PSR B1957+20 (= PSR J1959+2048) [61]. It is a binary that contains a 1.6 ms MSP and a very low mass companion ( $M_c \sim 0.02M_\odot$ ) in a 9.2 h orbit. Eclipses of radio pulsations have been observed from this system during the phases called inferior conjunction when its companion lies between the MSP and us. Eclipses result from the absorption or scattering of the radio signals from the pulsar by the dense ionized gas streaming off from its evaporating companion ([98–100]). Such system is dubbed black widows because the situation is similar to a female spider that devours its mate after mating.

While the pulsed emission is the defining characteristic of a pulsar, it only consumes a tiny fraction of the rotational energy of the neutron star. Even with the pulsed radiation across the whole electromagnetic spectrum summed up, it can hardly exceed a few tens of percents of a pulsar's spin-down power. Most of the rotational energy of the neutron stars is carried away by the relativistic pulsar wind outflows. While the pulsed emission originates within the magnetosphere, the wind region extends beyond the light cylinder. We can detect the presence of the wind through its interactions with surroundings. For the case of PSR B1957+20, the effect of its pulsar wind can be revealed in several ways.

PSR B1957+20 has a transverse velocity of  $v \sim 220$  km/s [1], which is found to be supersonic and a bow-shock nebula can be formed. The termination shock radius is determined by the balance between the wind particles and the interstellar medium at the head of the shock. Through the interactions with the shocked medium, the relativistic wind particles radiate synchrotron emissions as they trail behind the pulsar's motion. This results in a cometary-tail bow-shock morphology. Figure 3 shows the X-ray bow-shock nebula of PSR B1957+20 as observed by Chandra, which was firstly discovered by [101].

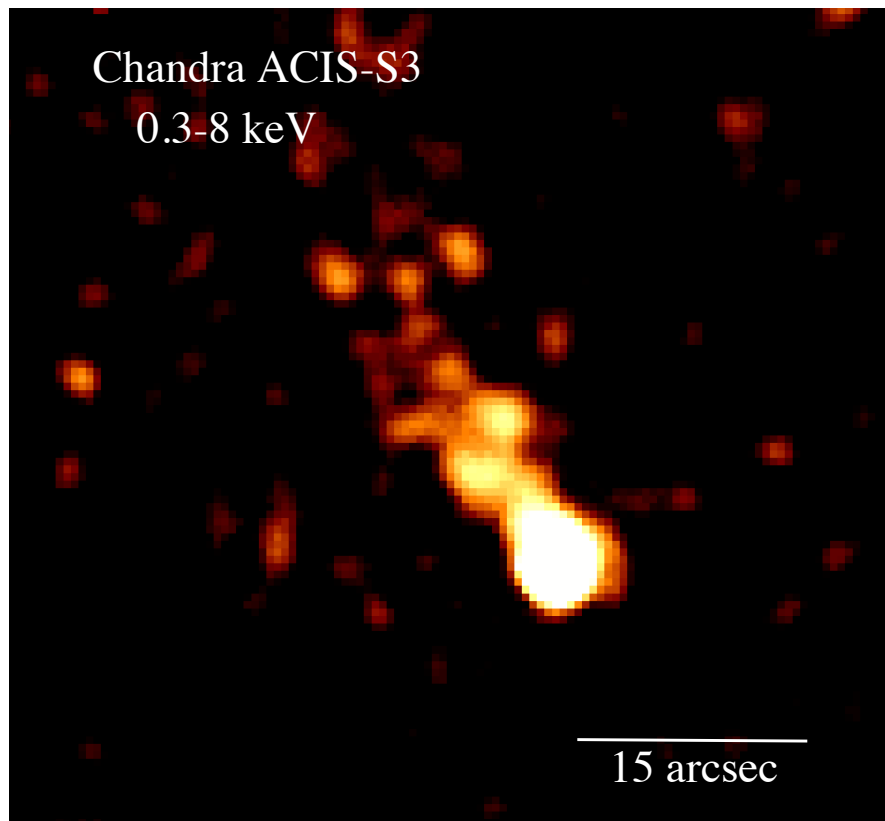


**Figure 3.** X-ray image of the bow-shock nebula associated with black widow MSP PSR B1957+20 obtained from the public data with an effective exposure of  $\sim 165$  ks as acquired by Chandra (Observation ID: 9088). This is the same data as used in the study by Huang et al. [63].

Systems of this kind can enable us to study the shock physics in the interstellar medium (ISM) [102]. The observed length  $l$  of the X-ray tail can be interpreted as the distance traversed by the pulsar within the electron synchrotron cooling timescale  $t_c$ , i.e.,  $l \sim v_p t_c$ , where  $v_p$  is the proper-motion velocity of the pulsar. The cooling time in the X-ray band is  $\sim 10^8 B_{\text{mG}}^{-3/2} (h\nu_X/\text{keV})^{-1/2}$  s, where  $B_{\text{mG}}$  is the inferred magnetic field strength in the emitting region [102]. Adopting the inferred tail length of  $\sim 9.7 \times 10^{17}$  cm at the distance of 2.5 kpc and a proper motion velocity of  $220 \text{ km s}^{-1}$ , the synchrotron cooling timescale is estimated to be  $\sim 4.9 \times 10^4$  yrs. This yields a magnetic field of  $B \sim 17.7 \mu\text{G}$  in the shock region. Considering a magnetic field strength of  $\sim 2\text{--}6 \mu\text{G}$  in the ISM, the compression factor of the magnetic field in the termination shock is estimated to be  $\sim 3$  [102].

Spatially-resolved spectroscopy can also shed light on the properties of the nebula [63]. For a synchrotron nebula powered by the MSP, a softening of the spectrum of the X-ray tail as a function of the distance from the pulsar is expected if synchrotron cooling of the particles injected at the termination shock is dominated. By dividing the tail into two segments, the photon index of the segment closer to the pulsar is found to be  $\Gamma \sim 1.6$  and that of the other is  $\Gamma \sim 2.1$  [63], which is consistent with the aforementioned scenario.

Currently, there are >70 pulsar wind nebulae detected in the X-ray [103]. However, only three of them are confirmed to be associated with MSPs (PSRs B1957+20 [101], J2124-3358 [104] and J1911-1114 [105]). We therefore encourage dedicated search into the archival X-ray imaging data, which can possibly reveal unreported faint X-ray nebulae associated with MSPs.

The interactions between the pulsar wind and the ablated material from its companion can also form intrabinary shock. Because of the geometry of the shock, this can lead to the modulation of high energy emissions across the orbit. In Figure 4, we show the X-ray light curve of PSR B1957+20 folded at the orbital period [63]. The observed flux is found to peak just before and just after the pulsar enters the radio eclipse region (the blue shaded regions). This can be interpreted as the Doppler boosting effect caused by the bulk flow in the downstream region.

The shock geometry is controlled by the ratio of the momentum fluxes of the pulsar wind to the stellar wind. For PSR B1957+20, such ratio is estimated to be  $\sim 10$  which suggests the companion star is confined by the pulsar wind and the shock [63]. The opening angle of the cone-like shock is  $\sim 50\text{--}60^\circ$ , which corresponds to a separation of  $\sim 0.15$  in orbital phase. Because the emission is concentrated in the forward direction of the flow, we therefore expect that double peaks due to the Doppler boosting effect appear at the  $\sim 0.15$  phase before and after the phase of the radio eclipse (i.e., inferior conjunction), which is consistent with the observed result (see Figure 4) [63].

Apart from X-ray, evidence for orbital modulation of this black widow MSP is also found in a  $\gamma$ -ray regime. The  $\gamma$ -ray emission of PSR B1957+20 at energies larger than 2.7 GeV has been found to be modulated at the orbital period [64] (see Figure 5). On the other hand, the emissions below 2.7 GeV are steady and are dominated by the pulsar emission. Figure 5 clearly shows that the enhanced emission above 2.7 GeV appears around the inferior conjunction. It has been speculated that the modulated GeV emission originates from the inverse-Compton scattering of the thermal radiation of the companion star off the “cold” (i.e., low energy of the leptons in the co-moving frame of the plasma) ultra-relativistic pulsar wind [64].

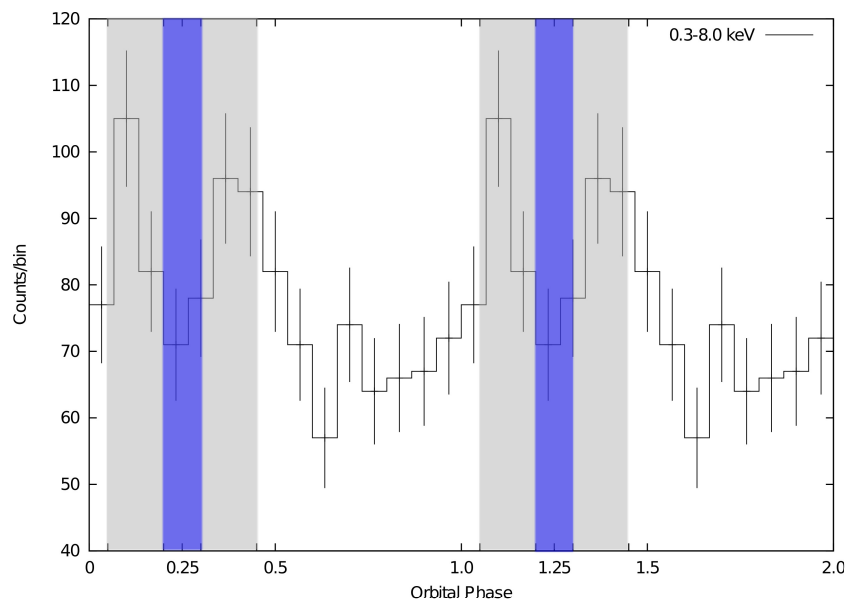


**Figure 4.** Orbital modulation of PSR B1957+20 in X-ray as observed by Chandra [63]. The error bars correspond to  $1\sigma$  uncertainties assuming Poisson noises. The eclipses of the radio pulses occur at the orbital phases of 0.2–0.3 and 1.2–1.3 which are highlighted by the blue regions. The grey regions represent the phases for extracting the X-ray spectrum of PSR B1957+20 in the eclipsing region in Huang et al. [63]. Two orbital cycles are shown for clarity.

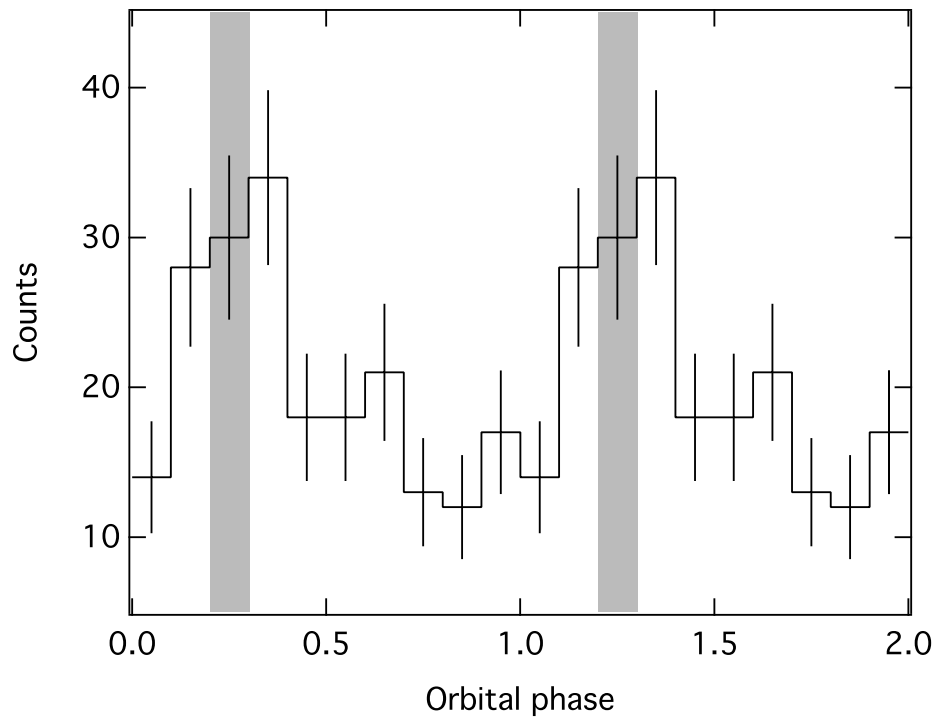


**Figure 5.**  $\gamma$ -ray orbital modulation of PSR B1957+20 observed by Fermi large area telescope (LAT). This is discovered by Wu et al. [64]. The error bars correspond to  $1\sigma$  uncertainties assuming Poisson noises. The shaded regions correspond to the phase of radio eclipse (i.e., 0.2–0.3 and 1.2–1.3). Two orbital cycles are shown for clarity.

Besides PSR B1957+20, only two other black widow MSPs (PSR J1311-3430 [45] and PSR J2241-5236 [72]) have their possible  $\gamma$ -ray modulations reported, which can possibly be a signature of intrabinary shock. However, their significance is not very high, including the prototypical case of PSR B1957+20. As more than 10 years of data have been accumulated by Fermi LAT, one can reexamine and check these  $\gamma$ -ray modulations together with the updated instrumental responses and the background model.

Currently, 27 black widows have been discovered in the galactic field (see Table 1) and 17 are found in globular clusters (Table 2). The companion stars in these systems are likely to degenerate and have masses  $\ll 0.1M_{\odot}$  [17,36]. For those in the galactic field, a number of them have their X-ray counterparts identified [20]. In Section 5, we will provide a general discussion on the X-ray and  $\gamma$ -ray natures of this population as a whole.

#### 4. Redbacks

Redbacks are close relatives of black widows, which are the other class of pulsar binaries that show intense interactions between the pulsars and the companion stars. They are named after the species of the poisonous spiders which originate from Australia. While the range of the orbital period spanned by these systems is similar to that of black widow MSPs ( $P_b \leq 20$  h), their companions are late-type non-degenerate stars with masses of  $M_c \sim 0.2 - 0.4M_{\odot}$  which are significantly higher than that of black widows ( $M_c \ll 0.1M_{\odot}$ ) [17].

Let us revisit the end stages of LMXB evolution. When a neutron star has been spun up sufficiently in the accretion-powered phase, particle acceleration can be re-initiated in its magnetosphere and the MSP is hence turned on [3]. However, the radio pulses cannot be observed unless the accretion disk and the dirty environment around it have been somehow cleared. Mechanisms involve processes such as pulsar wind ablation and radiation pressure from the MSP can possibly help to clear up

the environment [3,5]. However, the exact transition between the accretion-powered LMXB and the rotation-powered MSP has not been witnessed until a decade ago.

The first identified redback MSP, PSR J1023+0038, was initially identified as an LMXB FIRST J102347.6+003841 [106]. The source clearly showed an accretion disk before 2002 [107]. Since then, the disk was found to have disappeared. Subsequently, the radio pulsations have been detected in 2007 and PSR J1023+0038 revealed itself as a newly born MSP [27]. It is a long-sought missing piece in the evolutionary picture of compact X-ray binaries. Shortly after its discovery,  $\gamma$ -ray emission as well as the X-ray orbital modulation (see Figure 6) from PSR J1023+0038 have been subsequently detected [108].

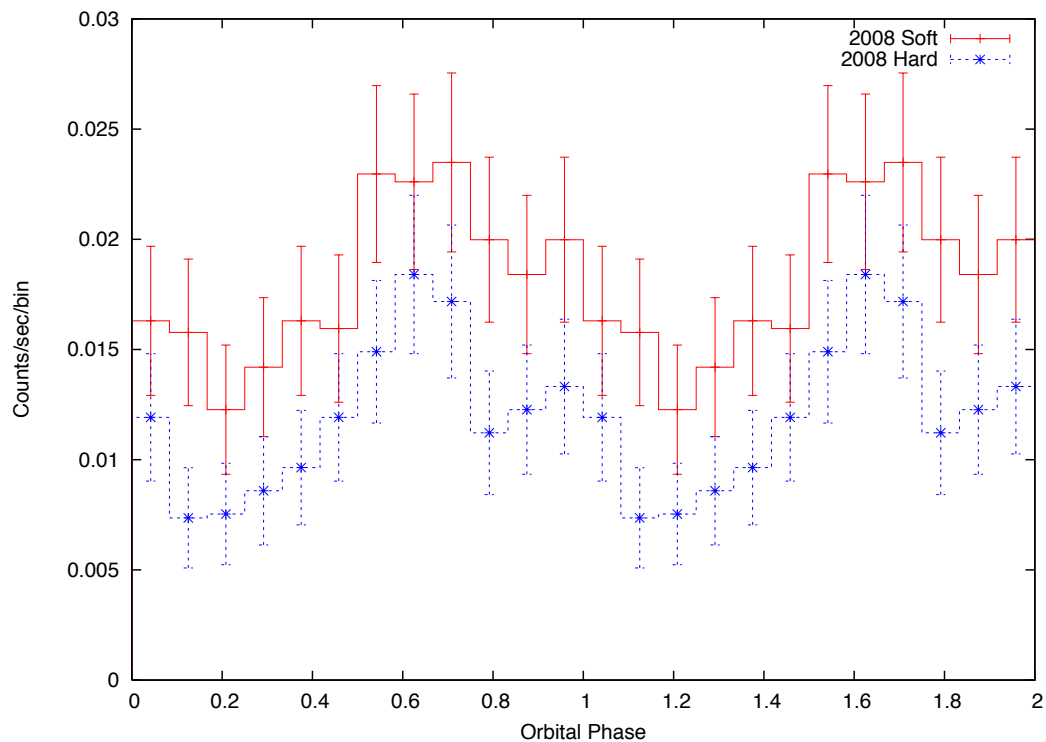


**Figure 6.** X-ray orbital modulation of PSR J1023+0038 in the soft (0.3–2.0 keV) and hard (2.0–10.0 keV) bands, as obtained from the observation taken at 26 November 2008 with XMM-Newton [108].

Interestingly, PSR J1023+0038 shows that MSP might not be just the end point in the evolution of compact binaries. Since 2013 late June, the radio pulsation of this system has disappeared ([109,110]) and a new accretion disk has been formed as shown by the re-appearance of strong double peaked  $H\alpha$  emission [111]. All this evidence indicate that this system was switching from a rotation-powered state back to an accretion-powered state.

Changes in all other wavelengths have been found to accompany this transition (see Figure 7) ([28,29]). First, its  $\gamma$ -rays suddenly brightened within a few days in 2013 June/July and have remained at a high  $\gamma$ -ray state. Second, both UV and X-ray fluxes have increased by roughly an order of magnitude. Moreover, the system does not show any X-ray orbital modulation after the transition.

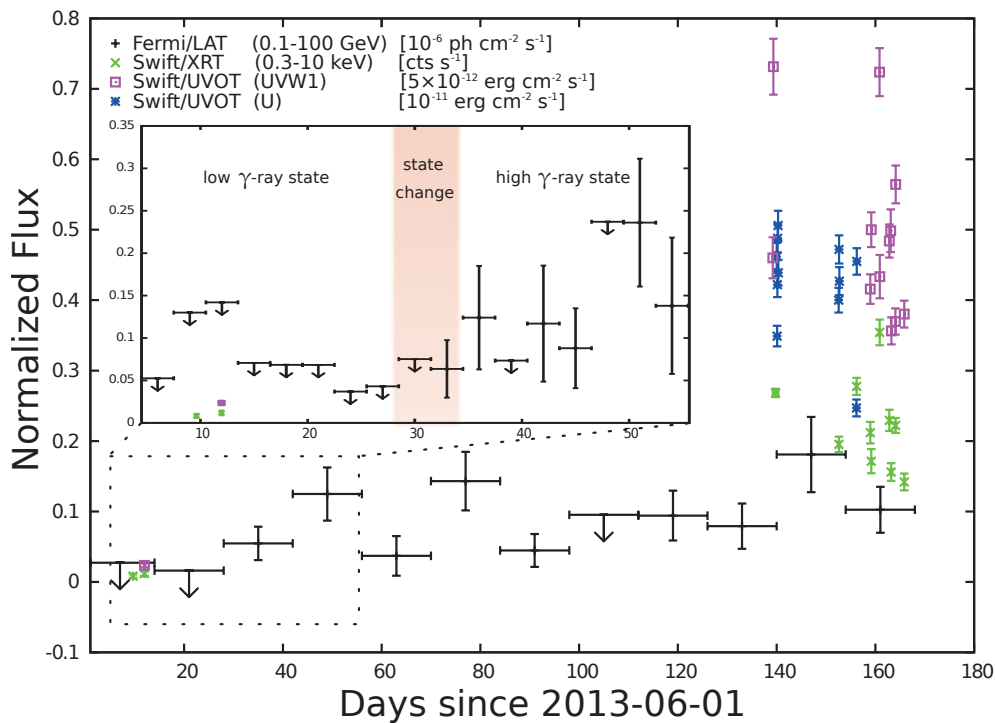


**Figure 7.** UV, X-ray and  $\gamma$ -ray lightcurves of PSR J1023+0038 from 1 June 2013 to 13 November 2013 are shown together in the main panel with different flux scales for each energy band (see upper left corner for details). On the other hand, the inset box shows the detailed evolution of the  $\gamma$ -ray emissions from 6 June to 24 July. Each data point of UV/X-ray represents an individual observation taken by Swift. Each  $\gamma$ -ray data points in the main panel and inset corresponds to two weeks and three days, respectively. In the cases where the detection significances is  $\leq 3\sigma$ , upper limits at 95% confidence are given instead [28].

Assuming the MSP is still active and the absence of radio pulsation is simply a result of absorption/scattering due to increased local charge density, the aforementioned multiwavelength behaviour of PSR J1023+0038 can be explained with the model illustrated in Figure 8 [28]. In this scenario, a new accretion disk was formed as a result of sudden increase of the stellar wind. This can provide an explanation for all the other observed phenomena after the transition.

The enhancement of the UV emission can be naturally accounted for by the newly formed disk. The increase of the  $\gamma$ -ray flux by an order of magnitude suggests that a new emission component emerges after the transition. We propose that the inverse-Compton scattering process of the cold-relativistic pulsar wind off the optical/UV photons from the accretion disk produces the additional  $\gamma$ -rays.

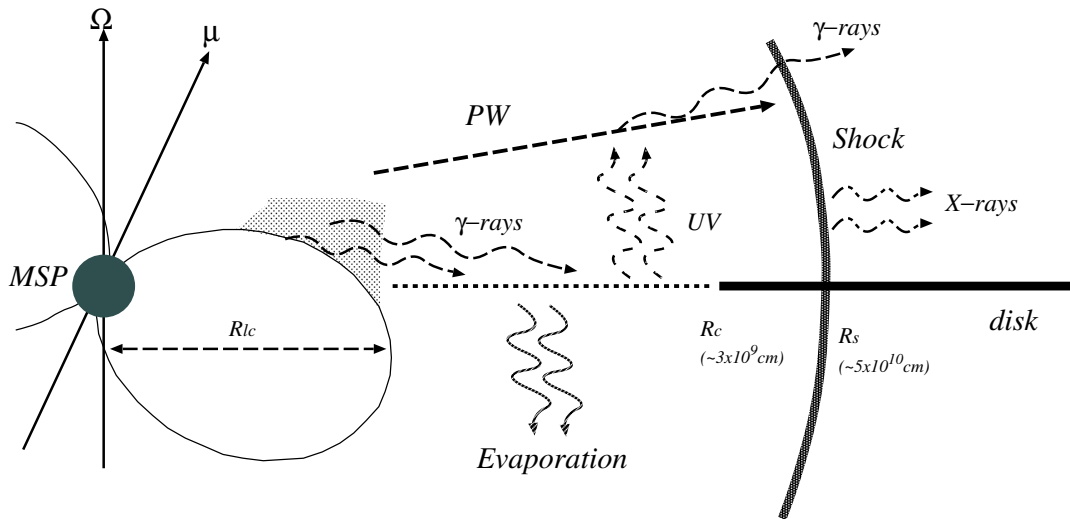


**Figure 8.** Schematic illustration for the emission nature of PSR J1023+0038 after 2013 late June in different wavelengths. The accretion disk extends beyond the light cylinder radius ( $R_{lc}$ ).  $R_s$  is the distance to the intra-binary shock from the pulsar.  $R_c$  is the critical distance from the pulsar at which the  $\gamma$ -rays from its magnetosphere evaporate the disk matter at  $R < R_c \sim 3 \times 10^9$  cm. UV/Optical photons mainly originate from the disk at  $R \sim 10^9-10^{10}$  cm. Shock is formed through the interaction between the pulsar wind and the stellar wind. This produces the non-thermal X-ray emissions. The inverse-Compton process of the cold-relativistic pulsar wind off UV/Optical photons from the disk produces the additional  $\gamma$ -rays [28].

Before the transition in June 2013, X-ray modulation was observed from PSR J1023+0038 where the emission originated from the intra-binary shock ([108,112]). It has been suggested that during the MSP phase, the emission region is closer to the companion star and its orbital variations are caused by the eclipse of the emission region by the companion star [112]. After the transition, it is possible that the size of the emission region is getting bigger than that of before late June 2013. In such a case, the companion star can only block a negligible fraction of this emission and hence this explains the disappearance of the orbital X-ray variation. It has been speculated that the increase in the mass transfer from the companion star pushes the emission region back toward the pulsar, and more fraction of the pulsar wind is stopped by the shock, resulting in an increase in the X-ray emissions from the system [28].

In Figure 9, the multiwavelength spectral energy distributions (SEDs) of PSR J1023+0038 before and after the transition in June 2013 are compared [28]. Moreover, the theoretical models based on the aforementioned scenario are overlaid on the observed data. It appears that this scenario proposed by [28] can explain the results quite well.

PSR J1023+0038 is an archetypal examples of a growing group of transitional MSPs (tMSPs). This includes PSR J1824-2452I, which resides in the globular cluster M28 [91]. Its X-ray counterpart is a transient IGR J1824-2452. In 2013, it was detected as an X-ray outburst with rotational and orbital ephemeris the same as PSR J1824-2452I. Interestingly, after a month long X-ray burst, the system was found to be reactivated as an active radio MSP within a few days. Another tMSP XSS J1227-4859 was previously identified as an LMXB with positional coincidence with Fermi LAT source 1FGL J1227.9-4852/2FGL J1227.7-4853 [113]. In December 2013, a transition was accompanied with a brightness drop in opticals, X-rays and  $\gamma$ -rays [114,115]. Radio searches at the beginning of 2014 eventually detected the pulses at 607 MHz from the system [116].

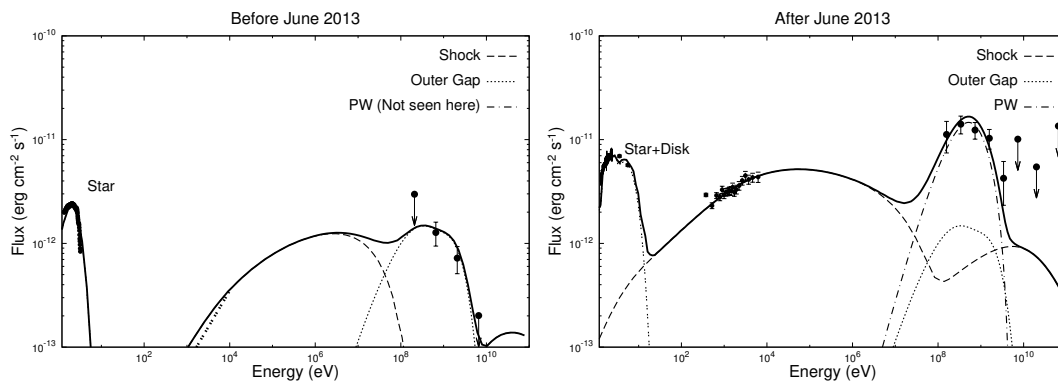


**Figure 9.** Multi-wavelength spectral energy distributions of a PSR J1023+0038 system before (**left**) and after (**right**) late June 2013. Calculations with a model consist of emission components from the pulsar magnetosphere (outer gap); shock and pulsar wind (PW) are compared with the observed data before and after the transition. For further details, please refer to [28].

tmSPs are not the only redback that show dramatic changes. Very recently, we observed another redback system PSR J1048+2339 with the Lulin 1 m telescope in Taiwan and 2 m Liverpool telescope in La Palma [34]. Its orbital modulation in the optical regime has been found to change drastically in a timescale of less than two weeks (see Figure 10). From the observations taken in March 2018, the optical light curve folded at the orbital period of 6 h resembles an ellipsoidal modulation of the companion star which shows two peaks in a cycle at  $\phi = 0$  and  $\phi = 0.55$ . Ellipsoidal modulation is a consequence of the orbital motion for a tidally distorted companion, which is commonly seen among redback systems (e.g., PSR J2129-0429 [117]). In Figure 10, the minimum at  $\phi = 0.25$  corresponds to the inferior conjunction.

When PSR J1048+2339 was observed again in early April 2018, its light curve was found to be completely different from that obtained in March (see Figure 10). It became a single-peaked sinusoidal profile with a maximum at  $\phi = 0.65$  and a minimum at  $\phi = 0.25$ . Furthermore, the brightness of the companion is increased by one magnitude. All this suggests the modulation is now dominated by pulsar wind heating of the companion [34]. The change from an ellipsoidal modulation to a brightened sinusoidal profile occurred in less than 14 days [34]. The irradiation power of the system has been found to increase by a factor of six, and it has been speculated that this is related to the activity of the companion star [34]. The magnetic field of the companion star could play an important role by connecting to the shock region and guides the pair plasmas to the companion star surface.

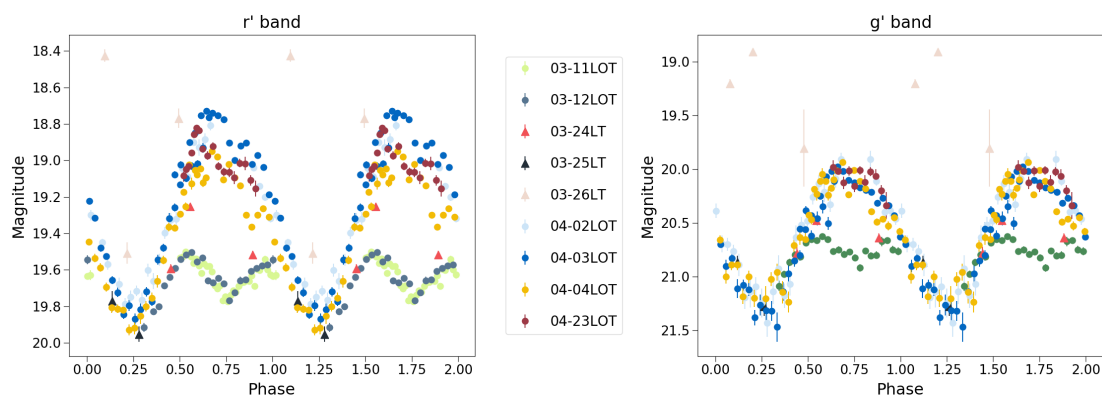


**Figure 10.** Light curves of PSR J1048+2339 companion star with  $r'$  and  $g'$  band filter, as observed by a 1 m Lulin telescope and a 2 m Liverpool telescope between 11 March 2018 and 23 April, folded with an orbital period of 6 h [34].

## 5. Population Analysis of Spider MSPs in High Energy

### 5.1. X-Ray Properties

As the number of MSPs have significantly enlarged over the last decade, it is possible to carry out a statistical analysis of their population as a whole and examine similarities and differences among various classes. Recently, the authors of Lee et al. [20] performed an X-ray census of all MSPs in the galactic field. By utilizing all the available X-ray data, 47 MSPs have their X-ray counterparts detected (see Table 1 in [20]). On the other hand, upper limits have been placed on the X-ray emission of another 36 MSPs (see Table 2 in [20]). Using this censored data, the authors of Lee et al. [20] examined the empirical relation between their X-ray luminosities  $L_x$  and spin-down power  $\dot{E}$  (see Figure 11). The best-fit relation is found to be  $L_x \simeq 10^{31.05} \dot{E}_{35}^{1.31}$  erg/s in 2–10 keV (i.e., the Akritas–Thiel–Sen (ATS) line in Figure 11 [20]), where  $\dot{E}$  is the spin-down power with units of  $10^{35}$  erg/s.

Concerning the spider pulsars, there are eight rebacks and 12 black widows in the X-ray selected sample adopted in the study by Lee et al. [20]. By comparing their physical properties with the non-spider MSPs, while the distributions of the surface magnetic field strengths among different classes are found to be similar, the magnetic field strength at the light cylinder as well as the spin-down powers of rebacks are found to be significantly higher than those of non-spider MSPs in binaries.

Comparing the rotational and orbital parameters of rebacks and black widows, there is no significant difference found [20]. However,  $L_x$  of rebacks are found to be significantly higher than those of black widows [20] (see Figure 12). Moreover, there is an indication that the X-ray emission of rebacks is harder than that of black widows [20] (see Figure 12).

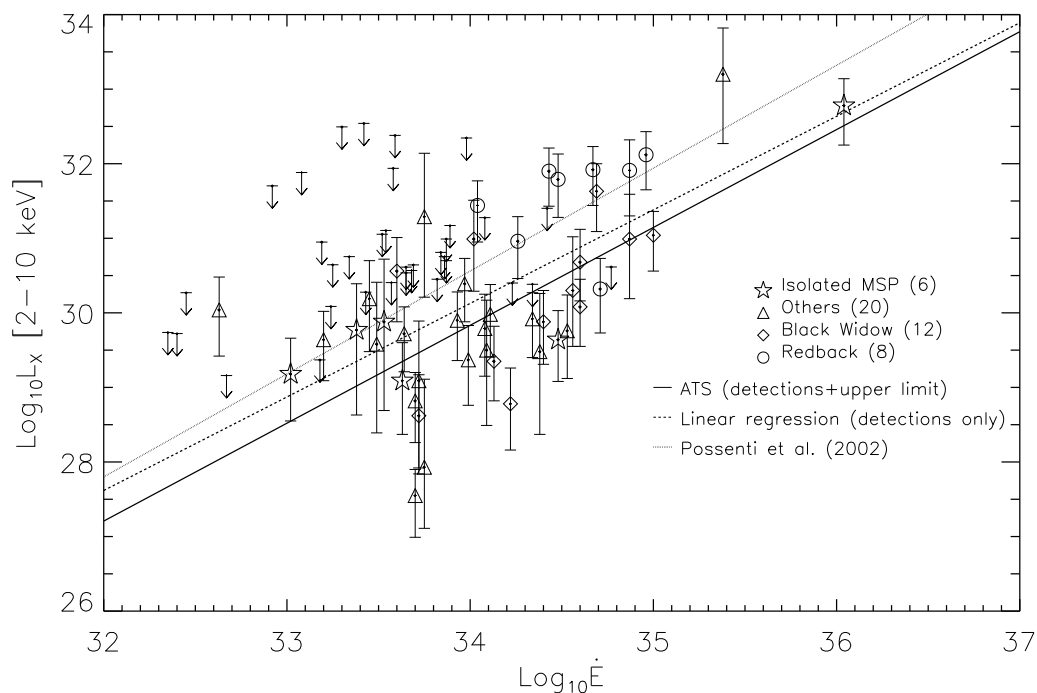


**Figure 11.** Relation between  $L_x$  and  $\dot{E}$  for 46 MSPs of different classes which are shown as different symbols in this plot [20]. In addition, the upper-limits on  $L_x$  for 35 MSPs are included in the sample with which Lee et al. [20] performed the survival analysis. The solid line illustrates the Akritas–Thiel–Sen (ATS) line inferred from this censored data. For comparison, the dashed line illustrates the result from the standard linear regression of X-ray detected MSPs. Moreover the relation reported by Possenti et al. [118] based on a sample of 10 MSPs is displayed as the dotted line [20].

The difference in their X-ray luminosities can be explained by the different contributions from their intrabinary shocks [20]. The shock luminosity is proportional to  $L_X \propto \delta \dot{E}$ , where  $\delta$  is the fraction of the pulsar wind blocked by the outflow from the companion star and/or the companion star itself.  $\delta$  can be estimated by the fraction of the sky intercepted by the companion star with  $\delta \sim (R_R/2a)^2$ , where  $R_R$  is the Roche-lobe radius of the companion star. Since the Roche-lobe radius is estimated as  $R_R/a = 0.462[q/(1+q)]^{1/3}$  with  $q$  being the ratio of the companion mass to the neutron star mass, the fraction can be expressed as  $\delta = 0.053[q/(1+q)]^{2/3}$ . With the typical values of the mass ratio for both classes of spider pulsars, Lee et al. [20] estimate  $\delta \sim 1\%$  for redbacks ( $q = 0.1$ ) and  $\delta \sim 0.2\%$  for black widows ( $q = 0.01$ ). This may explain their difference in  $L_X$ .

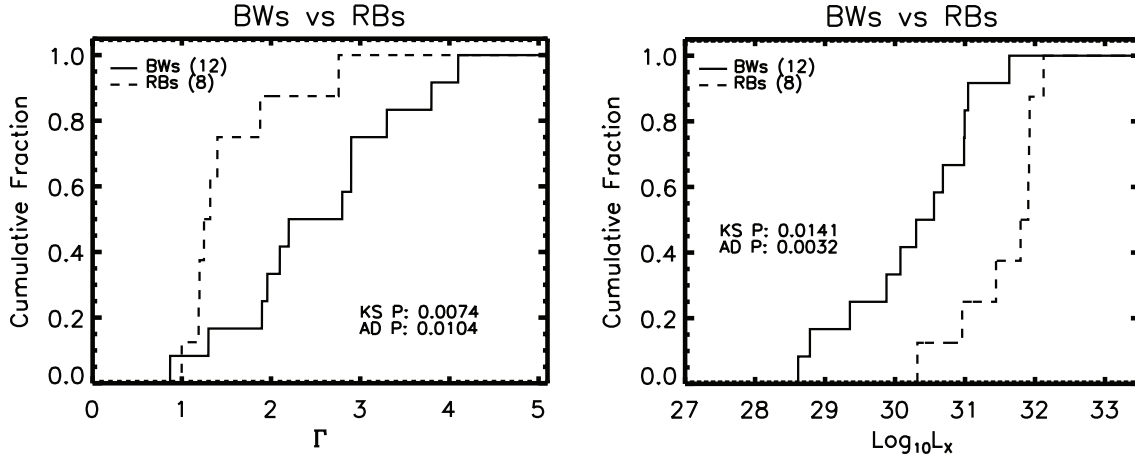


**Figure 12.** Comparison of the effective photon indices  $\Gamma$  of black-widows (BW) and redbacks (RB) in X-ray (left panel). The comparison of the X-ray luminosities  $L_x$  of BWs and RBs (right panel). The  $p$ -values resulting from the two-sample Kolmogorov–Smirnov (KS) test and Anderson–Darling (AD) test are given in each figure, and strongly indicate the differences between these two classes of MSPs [20].

## 5.2. $\gamma$ -Ray Properties

While the aforementioned work has investigated the X-ray properties of spider MSPs, there is no systematic analysis of their  $\gamma$ -ray properties that has been reported elsewhere. For a complete review on the high energy nature of these MSPs, we here present a statistical analysis of their  $\gamma$ -ray properties.

First, we investigate the  $L_\gamma - \dot{E}$  relation for the most updated sample of  $\gamma$ -ray pulsars, where  $L_\gamma$  is the  $\gamma$ -ray luminosity in 0.1–100 GeV. We make use of the Fermi LAT 8-Year Point Source Catalog (4FGL) of the version updated on 29 May 2019 [11]. Among 5065 sources detected at a significance above  $4\sigma$ , 239 of them are classified as pulsars. For computing their  $L_\gamma$  and  $\dot{E}$ , we need the estimates of their distance as well as  $\dot{P}$ . Searching for such properties of the 4FGL pulsars from the ATNF catalog [1], we obtain a sample of 169 pulsars with their  $L_\gamma$  and  $\dot{E}$  plotted in Figure 13. By fitting a linear model to  $\log L_\gamma$  and  $\log \dot{E}$ , we obtain a best-fit relation of

$$\log L_\gamma = (0.63 \pm 0.05) \log \dot{E} + (11.87 \pm 1.78) \quad (3)$$

with the uncertainties estimated by bootstrapping. We plot this relation as a straight line in Figure 13. The data points for the spider pulsars are highlighted by the coloured symbols. We found they follow the general  $L_\gamma - \dot{E}$  trend inferred from the entire  $\gamma$ -ray population.

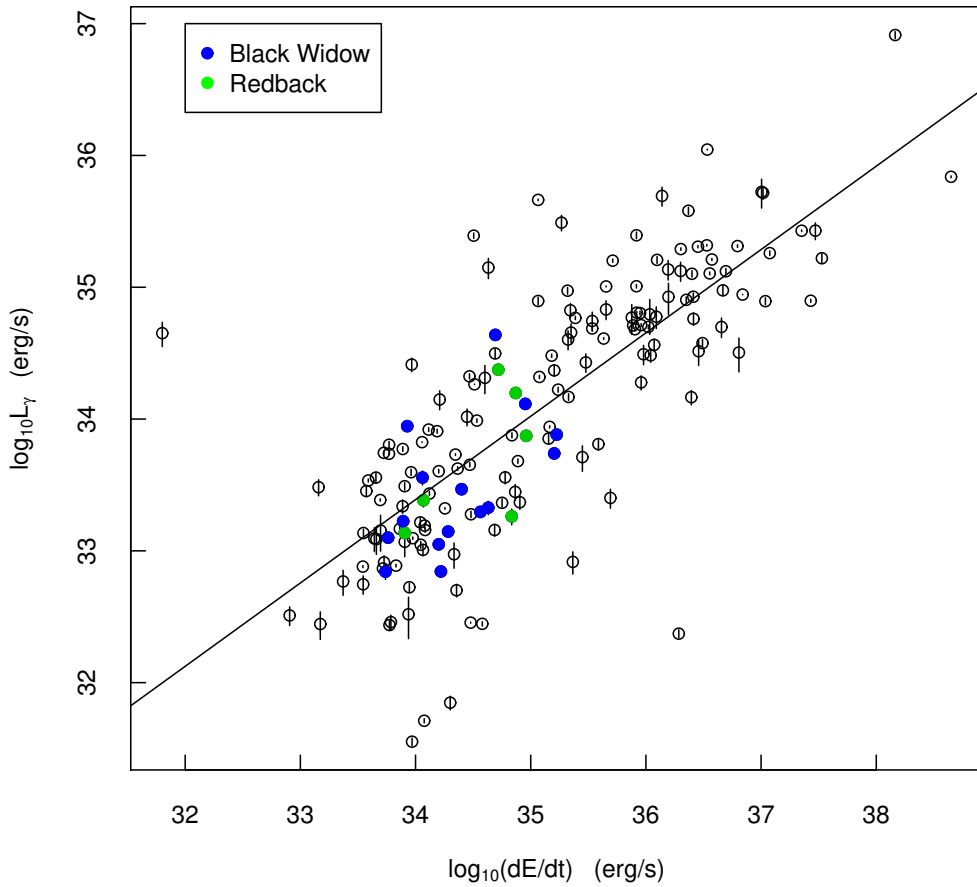


**Figure 13.** Plot of  $L_\gamma$  vs.  $\dot{E}$  for the  $\gamma$ -ray pulsars enlisted in the current version of the 4FGL catalog. The solid straight line illustrates the least square linear fit. The locations of black widows and redbacks in this parameter space are given by blue and green symbols, respectively.

Since the luminosities and the spectral properties of black widows and redbacks in X-ray regimes are found to be rather different [20], it is instructive to compare the corresponding properties of these two classes in  $\gamma$ -ray. The  $\gamma$ -ray spectrum of a pulsar is typically characterized by an exponentially cutoff power law with the following form:

$$\frac{dN}{dE} = K \left( \frac{E}{E_0} \right)^{-\Gamma} \exp \left( a \left( E_0^b - E^b \right) \right) \quad (4)$$

where  $E_0$  is a chosen energy scale expressed in MeV,  $K$  is the prefactor which describes the flux density of the pulsar,  $\Gamma$  is the photon index which describes the low energy spectral slope,  $a$  and  $b$  are the exponential factor and the exponential index which describe the cutoff at high energy. In the adopted 4FGL catalog, except for the six brightest  $\gamma$ -ray pulsars which were fitted with Equation (4) with  $b$  as free parameter, all the other pulsars are fitted with this function with  $b$  fixed at 2/3 [11].

In Figure 14, we construct the cumulative distribution functions for the  $\gamma$ -ray properties of black widows (blue symbols) and the redbacks (green symbols). We first compare  $L_\gamma$  of these two classes of spider MSPs (top left panel of Figure 14). In contrast to the case for X-rays, the distributions of  $L_\gamma$  of these two groups appear to be similar to each other. Applying a two-samples Anderson–Darling (A-D) test to their distribution, which is the same method adopted by [20] in comparing the X-ray properties of different classes of MSPs, we obtain a  $p$ -value of 0.6 and hence we conclude that there is no difference in the  $\gamma$ -ray luminosity distributions between black widows and redbacks. We have also compared the  $\dot{E}$  of this  $\gamma$ -ray selected sample (top right panel of Figure 14) and we also do not find any difference between black widows and redbacks.

In the lower-left and lower-right panels of Figure 14, we compare the distributions of  $\Gamma$  and  $a$  between the groups of 23 black widows and 10 redbacks from the 4FGL catalog. While these plots show some differences in their  $\gamma$ -ray spectral properties, A-D tests yield the  $p$ -values of 0.16 and 0.30 in comparing their distributions of  $\Gamma$  and  $a$ , respectively. Hence, we conclude that the  $\gamma$ -ray spectral properties of black widows and redbacks are consistent with each other.

In this analysis, we do not find any significant difference in the  $\gamma$ -ray properties between black widows and redbacks. The different contributions from the intrabinary shocks in these two MSP classes, which lead to their differences in the X-ray, do not result in any notable difference in the  $\gamma$ -ray regime. This suggests that the X-rays and  $\gamma$ -rays from these spider MSPs originated from different mechanisms. we conclude that the  $\gamma$ -ray emission of the spider pulsars are dominated by their magnetospheric radiation.

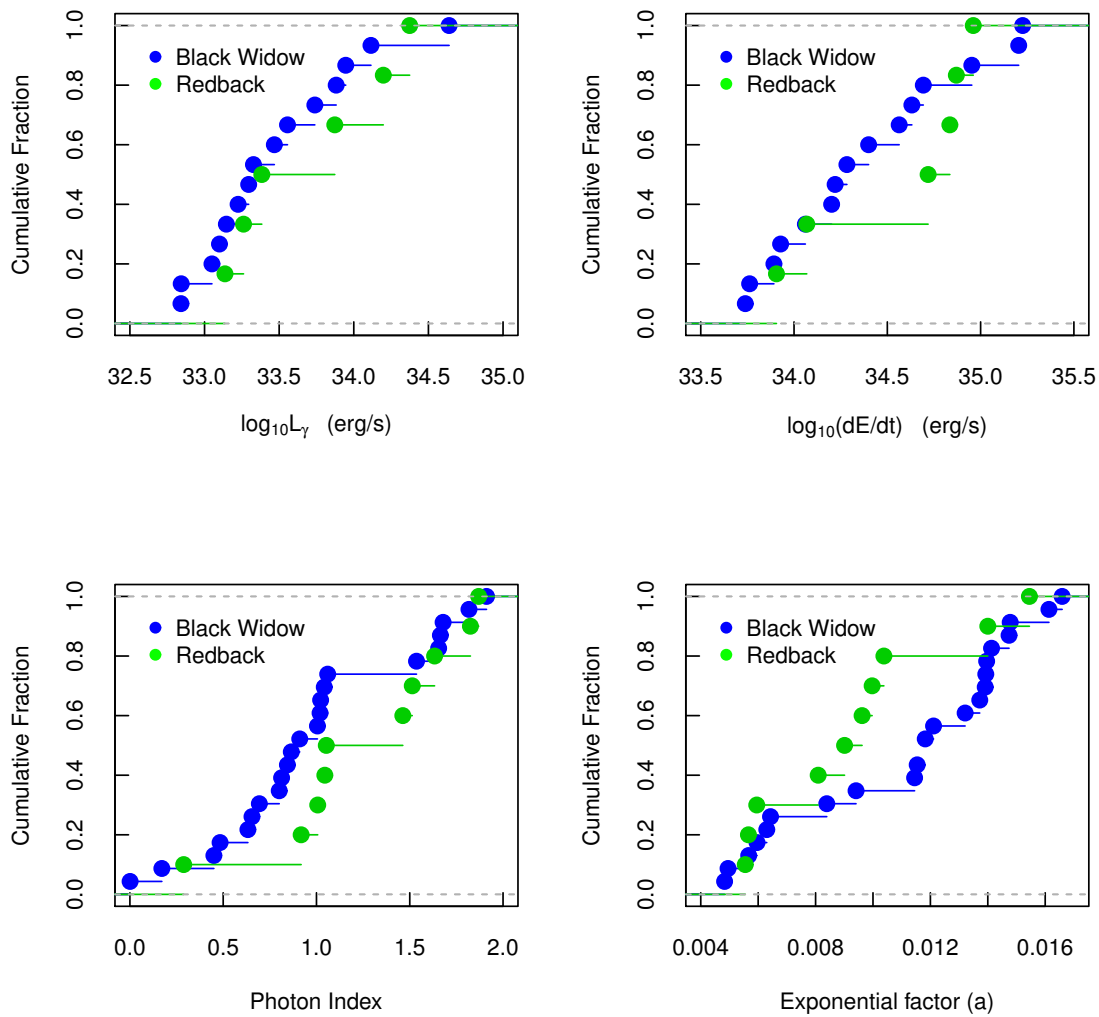


**Figure 14.** Comparisons of the step-wise empirical cumulative distributions of  $L_\gamma$  (upper-left panel),  $\dot{E}$  (upper-right panel),  $\gamma$ -ray photon index (lower-left panel) and  $\gamma$ -ray exponential factor  $a$  (lower-right panel) of black-widows and redbacks in  $\gamma$ -rays.

## 6. Future Prospects

We have seen that a vast of dramatic high energy phenomena have been observed from the spider MSPs. Here we would like to give a wish list for what kind of investigations we can do and what we can expect to learn from these targets in the near future.

1. Catch the changes in the act: PSR J1023+0038 is a classic example of a redback and demonstrates the swings between accretion-powered state and rotation-powered state. The emission properties of the

system have been found to change drastically along with the transition (Figures 7–9). Studying these variabilities can allow better understanding of the evolution of an LMXB in the recycling phase. However, it is impossible to catch such a transition without a long-term monitoring campaign. Almost all the spider pulsars are  $\gamma$ -ray emitters. Therefore, the continuous all-sky surveying mode of Fermi LAT provides us with the ideal instrument to monitor their behaviours. In Figure 15, we show the long-term  $\gamma$ -ray light curve of PSR J1023+0038 as observed by Fermi LAT. The transition in June 2013 (MJD 56450) can be clearly noted. Once a similar jump in the  $\gamma$ -ray flux has been spotted from any redbacks, a fast response X-ray/UV follow-up with the Neil Gehrels Swift Observatory can hence be triggered.

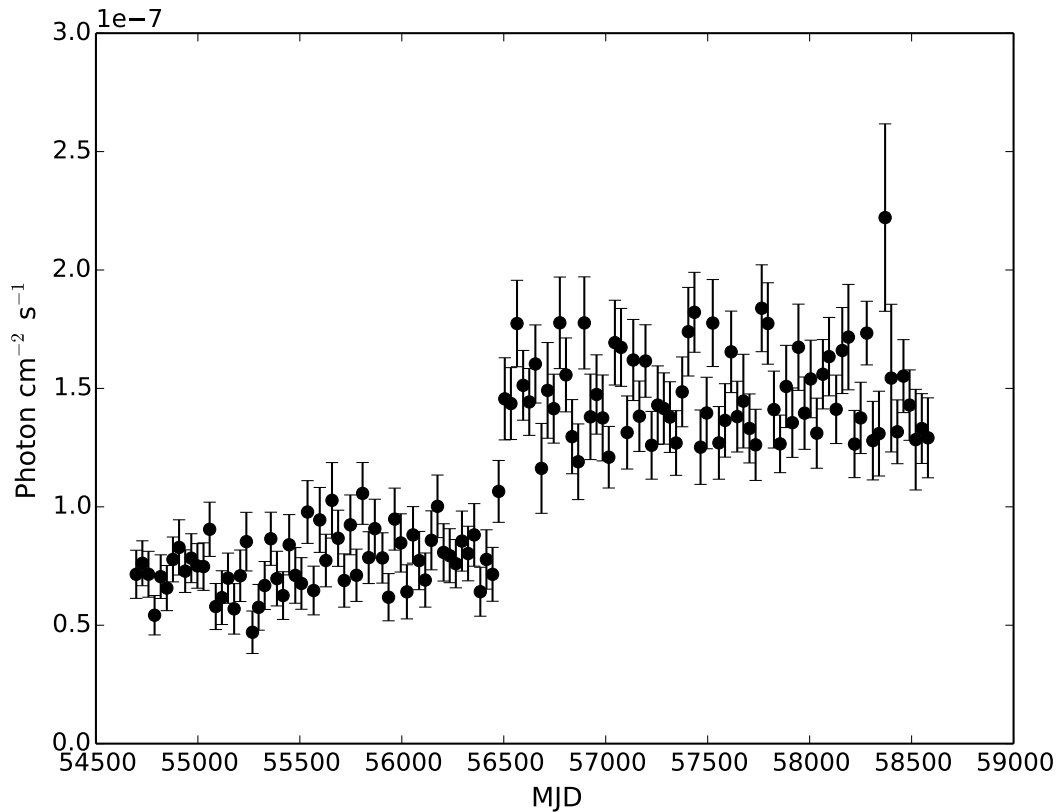


**Figure 15.** A long-term  $\gamma$ -ray light curve of PSR J1023+0038 as observed by Fermi LAT at energies  $> 100$  MeV from MJD 54697 (August 2008) to MJD 58580 (April 2019).

2. Globular clusters vs. Galactic field: In Section 5, we highlighted the results from the population analysis of the X-ray selected MSPs in the galactic field. We mentioned that the X-ray emission from the redbacks in the galactic field are apparently brighter and harder than the other classes of MSPs, including black widows (Figure 12). In Tables 1 and 2, we have shown that the current sample sizes of the spider pulsars in the galactic field and in globular clusters are comparable. The formation processes of MSPs in globular clusters is dynamical [119], which can be very different from those in galactic field. It is instructive to compare the rotational, orbital and emission properties between these two populations. As the properties of redbacks in the galactic field are found to be different from the other classes, it is interesting to see if their counterparts in globular clusters also share similar behaviours. One can also compare the redbacks/black widows in these two populations to explore if the dynamical formation processes in globular clusters can result in any difference.

3. Spider hunting: Thanks to Fermi, the MSP population has been significantly enlarged through the synergy of picking MSP-like candidates from the unidentified  $\gamma$ -ray sources and the multiwavelength identification campaign. In our previous MSP-like candidates selection, we adopt a simple set of selection criteria which was based on our current knowledge of MSPs (see Section 2).

However, the accuracy of picking the right candidates by this conventional method is unlikely to be optimal because the patterns in the data that define an MSP can be overlooked by human investigators. To improve the efficiency and the accuracy of the MSP identification campaign, machine learning techniques should be employed in  $\gamma$ -ray source classification.

We note that some studies have used such techniques to classify  $\gamma$ -ray sources (e.g., [120]). However, since the features for building the classification model were selected manually in these works, it is unlikely that the power of machine learning has been fully exploited. Recently, we have developed a scheme by coupling the classification algorithms with automatic feature extraction methods [121]. With this scheme, one can improve the prediction accuracy and pick the MSP-like  $\gamma$ -ray sources with higher confidence. Using the known  $\gamma$ -ray selected MSPs for testing our algorithm, we can attain an accuracy  $> 95\%$  in classifying MSPs while all the previous attempts can only achieve at most  $\sim 90\%$ . Therefore, we expect that the multiwavelength follow-up observations of the targets selected by this method can result in more spider pulsars.

Very recently, a new X-ray mission eROSITA was launched, on 13 July 2019.<sup>1</sup> eROSITA is equipped with seven identical Wolter-I mirror modules. Each module consists of 54 nested mirror shells. It is going to perform an all-sky survey in 0.3–10 keV with unprecedented sensitivity. Therefore, it will provide a full X-ray coverage of all unidentified  $\gamma$ -ray sources. On the other hand, the upcoming large synoptic survey telescope (LSST)<sup>2</sup> will have an 8.4 m mirror with an exceptionally wide field of  $3.5^\circ$ . It is capable of surveying the entire observable sky in the optical regime from its site in only three nights. It can provide deep multi-epoch data for the periodicity searches which enable us to identify the companions of the MSP-like objects.

In Table 3, we summarize the properties of a number of promising spider pulsar candidates. They were identified by the periodicities detected in X-ray/optical which resemble those orbital modulations found in redbacks/black widows. Three of these targets, 3FGL J0427.9–6704, FL8Y J1109.8–6500 and 3FGL J1544.6–1125, have shown stepwise jumps in their long-term X-ray light curves that are similar to the transitions between accretion-powered and rotation-powered states that have seen in PSR J1023+0038. Furthermore,  $H\alpha$  emissions have been detected from these three sources, which indicates the possibility of accretion. This makes them the candidates of tMSPs. Follow-up observations of them are strongly encouraged.<sup>3</sup>

**Table 3.** List of promising spider pulsar candidates.

Name	Orbital Period (day)	Mass Function ( $M_\odot$ )	X-ray Detection (Y/N)	Accretion (Y/N)	Modulation	References
3FGL J0212.1+5320	0.870	0.88	Y	N	Ox	[122,123]
3FGL J0427.9–6704	0.367	0.96	Y	Y	OXg	[124]
1FGL J0523.5–2529	0.688	0.49	Y	N	Og	[125,126]
3FGL J0744.1–2523	0.115		N	N	O	[127]
3FGL J0802.3–5610	0.416		Y	N	O	[127]
3FGL J0838.8–2829	0.215	0.69	Y	N	O	[128]
2FGL J0846.0+2820	8.133	0.14	N	Y?	o	[129]
3FGL J0954.8–3948	0.387	0.81	Y	N	Ox	[130]
FL8Y J1109.8–6500			Y	Y		[131]
3FGL J1544.6–1125	0.242	0.0015	Y	Y	O	[132,133]
2FGL J1653.6–0159	0.052	1.60	Y	N	Ox	[134,135]
3FGL J2039.6–5618	0.228	0.80	Y	N	OXg	[47,136–138]

O = Significant optical orbital modulation; o = Possible optical orbital modulation; X = Significant X-ray orbital modulation; x = Possible X-ray orbital modulation; g = Possible gamma-ray orbital modulation.

<sup>1</sup> <https://www.mpe.mpg.de/eROSITA>.

<sup>2</sup> <https://www.lsst.org>.

<sup>3</sup> We would like to point out that FL8Y J1109.8–6500 was enlisted in the preliminary catalogue with eight years of LAT data. However, it is excluded in the most recent version [11].

4. Push to very high energy regime: In a very high energy regime (VHE; >100 GeV), neither the pulsed emission nor the pulsar wind nebula has been detected from any MSP so far. However, the optical and X-ray modulations observed from spider MSPs indicate the presence of ablation and heating of their companions. The interaction of the pulsar and stellar winds can create a shocked region in which particles can be accelerated [139]. Such accelerated electrons can possibly Comptonize stellar radiation from the companion to the TeV energies. This process can produce orbital modulated VHE  $\gamma$ -rays.

On the other hand, black widow PSR B1957+20 has a bow-shock X-ray nebula (See Figure 3). Assuming the observed non-thermal X-ray emission up to  $\sim 10$  keV is produced in a synchrotron process, this implies the magnetic field of the nebula of the order of  $\mu\text{G}$  and the presence of high energy electrons with energies up to the order of a hundred TeV [102]. These electrons can also possibly Comptonize the ambient soft photon fields and result in VHE  $\gamma$ -rays [140]. It is interesting to note that the limiting fluxes in the TeV regime placed by MAGIC are very close to the theoretically predicted values (see Figure 8 in [141]).

Cherenkov telescope array (CTA) is the next generation VHE observatory which consists of more than 100 telescopes located in both the northern and southern hemispheres. Upon completion of the construction of the full array, CTA will have a much larger collecting area, wider energy coverage and a larger field-of-view than any existing VHE-observing facility. With its unprecedented performance at such high energies, it is not unreasonable to speculate that a number of spider pulsars can be detected in the VHE regime. This will open a new window for us to study these MSPs and help us to further constrain the acceleration processes of leptons within the binaries and their surrounding.

**Author Contributions:** The two authors contributed equally.

**Funding:** This research was funded by the National Research Foundation of Korea through grant numbers 2016R1A5A1013277 and 2019R1F1A1062071.

**Acknowledgments:** C.Y.H. is supported by the National Research Foundation of Korea through grants 2016R1A5A1013277 and 2019R1F1A1062071. K.L.L. is supported by the Ministry of Science and Technology of Taiwan through grant 108-2112-M-007-025-MY3.

**Conflicts of Interest:** The authors declare no conflict of interest.

## References

1. Manchester, R.N.; Hobbs, G.B.; Teoh, A.; Hobbs, M. The Australia Telescope National Facility Pulsar Catalogue. *Astron. J.* **2005**, *129*, 1993–2006. [[CrossRef](#)]
2. Zhang, B.; Harding, A.K.; Muslimov, A.G. Radio Pulsar Death Line Revisited: Is PSR J2144-3933 Anomalous? *Astrophys. J.* **2000**, *531*, L135–L138. [[CrossRef](#)] [[PubMed](#)]
3. Alpar, M.A.; Cheng, A.F.; Ruderman, M.A.; Shaham, J. A new class of radio pulsars. *Nature* **1982**, *300*, 728–730. [[CrossRef](#)]
4. Konar, S. The magnetic fields of millisecond pulsars in globular clusters. *Mon. Not. R. Astron. Soc.* **2010**, *409*, 259–268. [[CrossRef](#)]
5. Backer, D.C.; Kulkarni, S.R.; Heiles, C.; Davis, M.M.; Goss, W.M. A millisecond pulsar. *Nature* **1982**, *300*, 615–618. [[CrossRef](#)]
6. Hewish, A.; Bell, S.J.; Pilkington, J.D.H.; Scott, P.F.; Collins, R.A. Observation of a Rapidly Pulsating Radio Source. *Nature* **1968**, *217*, 709–713. [[CrossRef](#)]
7. Lorimer, D.R.; Faulkner, A.J.; Lyne, A.G.; Manchester, R.N.; Kramer, M.; McLaughlin, M.A.; Hobbs, G.; Possenti, A.; Stairs, I.H.; Camilo, F.; et al. The Parkes Multibeam Pulsar Survey—VI. Discovery and timing of 142 pulsars and a Galactic population analysis. *Mon. Not. R. Astron. Soc.* **2006**, *372*, 777–800. [[CrossRef](#)]
8. Keith, M.J.; Eatough, R.P.; Lyne, A.G.; Kramer, M.; Possenti, A.; Camilo, F.; Manchester, R.N. Discovery of 28 pulsars using new techniques for sorting pulsar candidates. *Mon. Not. R. Astron. Soc.* **2009**, *395*, 837–846. [[CrossRef](#)]

9. Manchester, R.N.; Lyne, A.G.; Camilo, F.; Bell, J.F.; Kaspi, V.M.; D'Amico, N.; McKay, N.P.F.; Crawford, F.; Stairs, I.H.; Possenti, A.; et al. The Parkes multi-beam pulsar survey—I. Observing and data analysis systems, discovery and timing of 100 pulsars. *Mon. Not. R. Astron. Soc.* **2001**, *328*, 17–35. [[CrossRef](#)]
10. Hui, C.Y. A Golden Decade of Gamma-Ray Pulsar Astronomy. *J. Korean Astron. Soc.* **2018**, *51*, 171–183
11. Abdollahi, S.; Acero, F.; Ackermann, M.; Ajello, M.; Atwood, W.B.; Axelsson, M.; Baldini, L.; Ballet, J.; Barbiellini, G.; Bastieri, D.; et al. Fermi Large Area Telescope Fourth Source Catalog. *arXiv* **2019**, arXiv:1902.10045v3.
12. Hui, C.Y.; Park, S.M.; Hu, C.P.; Lin, L.C.C.; Li, K.L.; Kong, A.K.H.; Tam, P.H.T.; Takata, J.; Cheng, K.S.; Jin, R.; et al. Searches for Millisecond Pulsar Candidates among the Unidentified Fermi Objects. *Astrophys. J.* **2015**, *809*, 68. [[CrossRef](#)]
13. Abdo, A.A.; Ackermann, M.; Ajello, M.; Atwood, W.B.; Axelsson, M.; Baldini, L.; Ballet, J.; Band, D.L.; Barbiellini, G.; Bastieri, D.; et al. Fermi/Large Area Telescope Bright Gamma-Ray Source List. *Astrophys. J. Suppl. Ser.* **2009**, *183*, 46–66. [[CrossRef](#)]
14. Romani, R.W.; Shaw, M.S. The Orbit and Companion of Probable  $\gamma$ -Ray Pulsar J2339-0533. *Astrophys. J. Lett.* **2011**, *743*, L26. [[CrossRef](#)]
15. Kong, A.K.H.; Huang, R.H.H.; Cheng, K.S.; Takata, J.; Yatsu, Y.; Cheung, C.C.; Donato, D.; Lin, L.C.C.; Kataoka, J.; Takahashi, Y.; et al. Discovery of an Unidentified Fermi Object as a Black Widow-like Millisecond Pulsar. *Astrophys. J. Lett.* **2012**, *747*, L3. [[CrossRef](#)]
16. Ray, P.S.; Belfiore, A.M.; Saz Parkinson, P.; Polisensky, E.; Ransom, S.M.; Romani, R.W.; Hessels, J.; Razzano, M.; Bhattacharyya, B.; Roy, J.; et al. Discovery of the radio and gamma-ray pulsar PSR J2339-0533 associated with the Fermi LAT bright source 0FGL J2339.8-0530. In *American Astronomical Society, AAS Meeting #223*; id.140.07; American Astronomical Society: Washington, DC, USA, 2014.
17. Roberts, M.S.E. Surrounded by spiders! New black widows and redbacks in the galactic field. *Proc. Int. Astron. Union* **2013**, *291*, 127–132. [[CrossRef](#)]
18. Arzoumanian, Z.; Brazier, A.; Burke-Spolaor, S.; Chamberlin, S.; Chatterjee, S.; Christy, B.; Cordes, J.M.; Cornish, N.J.; Crawford, F.; Thankful Cromartie, H.; et al. The NANOGrav 11-year Data Set: High-precision Timing of 45 Millisecond Pulsars. *Astrophys. J. Suppl. Ser.* **2018**, *235*, 37. [[CrossRef](#)]
19. Breton, R.P.; van Kerkwijk, M.H.; Roberts, M.S.E.; Hessels, J.W.T.; Camilo, F.; McLaughlin, M.A.; Ransom, S.M.; Ray, P.S.; Stairs, I.H. Discovery of the Optical Counterparts to Four Energetic Fermi Millisecond Pulsars. *Astrophys. J. Suppl. Ser.* **2013**, *769*, 108. [[CrossRef](#)]
20. Lee, J.; Hui, C.Y.; Takata, J.; Kong, A.K.H.; Tam, P.H.T.; Cheng, K.S. X-ray Census of Millisecond Pulsars in the Galactic Field. *Astrophys. J.* **2018**, *864*, 23 [[CrossRef](#)]
21. Cromartie, H.T.; Camilo, F.; Kerr, M.; Deneva, J.S.; Ransom, S.M.; Ray, P.S.; Ferrara, E.C.; Michelson, P.F.; Wood, K.S. Six New Millisecond Pulsars from Arecibo Searches of Fermi Gamma-Ray Sources. *Astrophys. J.* **2016**, *819*, 34. [[CrossRef](#)]
22. Draghis, P.; Romani, R.W.; Filippenko, A.V.; Brink, T.G.; Zheng, W.; Halpern, J.P.; Camilo, F. Multiband Optical Light Curves of Black-widow Pulsars. *Astrophys. J.* **2019**, *883*, 108. [[CrossRef](#)]
23. Burgay, M.; Joshi, B.C.; D'Amico, N.; Possenti, A.; Lyne, A.G.; Manchester, R.N.; McLaughlin, M.A.; Kramer, M.; Camilo, F.; Freire, P.C.C. The Parkes High-Latitude pulsar survey. *Mon. Not. R. Astron. Soc.* **2006**, *368*, 283–292. [[CrossRef](#)]
24. Pallanca, C.; Mignani, R.P.; Dalessandro, E.; Ferraro, F.R.; Lanzoni, B.; Possenti, A.; Burgay, M.; Sabbi, E. The Identification of the Optical Companion to the Binary Millisecond Pulsar J0610-2100 in the Galactic Field. *Astrophys. J.* **2012**, *755*, 180. [[CrossRef](#)]
25. Bassa, C.G.; Pleunis, Z.; Hessels, J.W.T.; Ferrara, E.C.; Breton, R.P.; Gusinskaia, N.V.; Kondratiev, V.I.; Sanidas, S.; Nieder, L.; Clark, C.J.; et al. LOFAR Discovery of the Fastest-spinning Millisecond Pulsar in the Galactic Field. *Astrophys. J. Lett.* **2017**, *846*, L20. [[CrossRef](#)]
26. Ho, W.C.G.; Heinke, C.O.; Chugunov, A.I. XMM-Newton Detection and Spectrum of the Second Fastest Spinning Pulsar PSR J0952–0607. *Astrophys. J.* **2019**, *882*, 128. [[CrossRef](#)]
27. Archibald, A.M.; Stairs, I.H.; Ransom, S.M.; Kaspi, V.M.; Kondratiev, V.I.; Lorimer, D.R.; McLaughlin, M.A.; Boyles, J.; Hessels, J.W.T.; Lynch, R.; et al. A Radio Pulsar/X-ray Binary Link. *Science* **2009**, *324*, 1411–1414. [[CrossRef](#)]

28. Takata, J.; Li, K.L.; Leung, G.C.K.; Kong, A.K.H.; Tam, P.H.T.; Hui, C.Y.; Wu, E.M.H.; Xing, Y.; Cao, Y.; Tang, S.; et al. Multi-wavelength Emissions from the Millisecond Pulsar Binary PSR J1023+0038 during an Accretion Active State. *Astrophys. J.* **2014**, *785*, 131. [[CrossRef](#)]
29. Li, K.L.; Kong, A.K.H.; Takata, J.; Cheng, K.S.; Tam, P.H.T.; Hui, C.Y.; Jin, R. NuSTAR Observations and Broadband Spectral Energy Distribution Modeling of the Millisecond Pulsar Binary PSR J1023+0038. *Astrophys. J.* **2014**, *797*, 111. [[CrossRef](#)]
30. Xing, Y.; Wang, Z.X.; Takata, J. Possible modulated  $\gamma$ -ray emission from the transitional millisecond pulsar binary PSR J1023+0038. *Res. Astron. Astrophys.* **2018**, *18*, 127. [[CrossRef](#)]
31. Archibald, A.M.; Bogdanov, S.; Patruno, A.; Hessels, J.W.T.; Deller, A.T.; Bassa, C.; Janssen, G.H.; Kaspi, V.M.; Lyne, A.G.; Stappers, B.W.; et al. Accretion-powered Pulsations in an Apparently Quiescent Neutron Star Binary. *Astrophys. J.* **2015**, *807*, 62. [[CrossRef](#)]
32. Ambrosino, F.; Papitto, A.; Stella, L.; Meddi, F.; Cretaro, P.; Burderi, L.; Di Salvo, T.; Israel, G.L.; Ghedina, A.; Di Fabrizio, L.; et al. Optical pulsations from a transitional millisecond pulsar. *Nat. Astron.* **2017**, *1*, 854. [[CrossRef](#)]
33. Cho, P.B.; Halpern, J.P.; Bogdanov, S. Variable Heating and Flaring of Three Redback Millisecond Pulsar Companions. *Astrophys. J.* **2018**, *866*, 71. [[CrossRef](#)]
34. Yap, Y.X.; Li, K.L.; Kong, A.K.H.; Takata, J.; Lee, J.; Hui, C.Y. Face changing companion of the redback millisecond pulsar PSR J1048+2339. *Astron. Astrophys.* **2019**, *621*, L9. [[CrossRef](#)]
35. Hessels, J.W.T.; Roberts, M.S.E.; McLaughlin, M.A.; Ray, P.S.; Bangale, P.; Ransom, S.M.; Kerr, M.; Camilo, F.; Decesar, M.E. A 350-MHz GBT Survey of 50 Faint Fermi  $\gamma$ -ray Sources for Radio Millisecond Pulsars. In *American Institute of Physics Conference Series*; Burgay, M., D'Amico, N., Esposito, P., Pellizzoni, A., Possenti, A., Eds.; American Institute of Physics: New York, NY, USA, 2011; Volume 1357, pp. 40–43. [[CrossRef](#)]
36. Gentile, P.A.; Roberts, M.S.E.; McLaughlin, M.A.; Camilo, F.; Hessels, J.W.T.; Kerr, M.; Ransom, S.M.; Ray, P.S.; Stairs, I.H. X-ray Observations of Black Widow Pulsars. *Astrophys. J.* **2014**, *783*, 69. [[CrossRef](#)]
37. Roy, J.; Ray, P.S.; Bhattacharyya, B.; Stappers, B.; Chengalur, J.N.; Deneva, J.; Camilo, F.; Johnson, T.J.; Wolff, M.; Hessels, J.W.T.; et al. Discovery of PSR J1227-4853: A Transition from a Low-mass X-ray Binary to a Redback Millisecond Pulsar. *Astrophys. J. Lett.* **2015**, *800*, L12. [[CrossRef](#)]
38. de Martino, D.; Casares, J.; Mason, E.; Buckley, D.A.H.; Kotze, M.M.; Bonnet-Bidaud, J.M.; Mouchet, M.; Coppejans, R.; Gulbis, A.A.S. Unveiling the redback nature of the low-mass X-ray binary XSS J1227.0-4859 through optical observations. *Mon. Not. R. Astron. Soc.* **2014**, *444*, 3004–3014. [[CrossRef](#)]
39. Xing, Y.; Wang, Z. Fermi Observation of the Transitional Pulsar Binary XSS J12270-4859. *Astrophys. J.* **2015**, *808*, 17. [[CrossRef](#)]
40. Papitto, A.; de Martino, D.; Belloni, T.M.; Burgay, M.; Pellizzoni, A.; Possenti, A.; Torres, D.F. X-ray coherent pulsations during a sub-luminous accretion disc state of the transitional millisecond pulsar XSS J12270-4859. *Mon. Not. R. Astron. Soc.* **2015**, *449*, 26. [[CrossRef](#)]
41. Ray, P.S.; Abdo, A.A.; Parent, D.; Bhattacharya, D.; Bhattacharyya, B.; Camilo, F.; Cognard, I.; Theureau, G.; Ferrara, E.C.; Harding, A.K.; et al. Radio Searches of Fermi LAT Sources and Blind Search Pulsars: The Fermi Pulsar Search Consortium. *arXiv* **2012**, arXiv:1205.3089.
42. Li, M.; Halpern, J.P.; Thorstensen, J.R. Optical Counterparts of Two Fermi Millisecond Pulsars: PSR J1301+0833 and PSR J1628-3205. *Astrophys. J.* **2014**, *795*, 115. [[CrossRef](#)]
43. Pletsch, H.J.; Guillemot, L.; Allen, B.; Kramer, M.; Aulbert, C.; Fehrmann, H.; Ray, P.S.; Barr, E.D.; Belfiore, A.; Camilo, F.; et al. Discovery of Nine Gamma-Ray Pulsars in Fermi Large Area Telescope Data Using a New Blind Search Method. *Astrophys. J.* **2012**, *744*, 105. [[CrossRef](#)]
44. Romani, R.W.; Filippenko, A.V.; Silverman, J.M.; Cenko, S.B.; Greiner, J.; Rau, A.; Elliott, J.; Pletsch, H.J. PSR J1311-3430: A Heavyweight Neutron Star with a Flyweight Helium Companion. *Astrophys. J. Lett.* **2012**, *760*, L36. [[CrossRef](#)]
45. Xing, Y.; Wang, Z. Discovery of Gamma-Ray Orbital Modulation in the Black Widow PSR J1311-3430. *Astrophys. J. Lett.* **2015**, *804*, L33. [[CrossRef](#)]
46. Bates, S.D.; Thornton, D.; Bailes, M.; Barr, E.; Bassa, C.G.; Bhat, N.D.R.; Burgay, M.; Burke-Spolaor, S.; Champion, D.J.; Flynn, C.M.L.; et al. The High Time Resolution Universe survey-XI. Discovery of five recycled pulsars and the optical detectability of survey white dwarf companions. *Mon. Not. R. Astron. Soc.* **2015**, *446*, 4019–4028. [[CrossRef](#)]

47. Strader, J.; Swihart, S.; Chomiuk, L.; Bahramian, A.; Britt, C.; Cheung, C.C.; Dage, K.; Halpern, J.; Li, K.L.; Mignani, R.P.; et al. Optical Spectroscopy and Demographics of Redback Millisecond Pulsar Binaries. *Astrophys. J.* **2019**, *872*, 42. [[CrossRef](#)]
48. Ng, C.; Bailes, M.; Bates, S.D.; Bhat, N.D.R.; Burgay, M.; Burke-Spolaor, S.; Champion, D.J.; Coster, P.; Johnston, S.; Keith, M.J.; et al. The High Time Resolution Universe pulsar survey—X. Discovery of four millisecond pulsars and updated timing solutions of a further 12. *Mon. Not. R. Astron. Soc.* **2014**, *439*, 1865–1883. [[CrossRef](#)]
49. Sanpa-arsa, S. Searching for New Millisecond Pulsars with the Gbt in Fermi Unassociated Sources. Ph.D Thesis, University of Virginia, Charlottesville, VA, USA, 2016.
50. Bhattacharyya, B.; Roy, J.; Ray, P.S.; Gupta, Y.; Bhattacharya, D.; Romani, R.W.; Ransom, S.M.; Ferrara, E.C.; Wolff, M.T.; Camilo, F.; et al. GMRT Discovery of PSR J1544+4937: An Eclipsing Black-widow Pulsar Identified with a Fermi-LAT Source. *Astrophys. J. Lett.* **2013**, *773*, L12. [[CrossRef](#)]
51. Tang, S.; Kaplan, D.L.; Phinney, E.S.; Prince, T.A.; Breton, R.P.; Bellm, E.; Bildsten, L.; Cao, Y.; Kong, A.K.H.; Perley, D.A.; et al. Identification of the Optical Counterpart of Fermi Black Widow Millisecond Pulsar PSR J1544+4937. *Astrophys. J. Lett.* **2014**, *791*, L5. [[CrossRef](#)]
52. Lorimer, D. All Published and Unpublished Millisecond Pulsars Not Associated with a Globular Cluster. Available online: <http://astro.phys.wvu.edu/GalacticMSPs/GalacticMSPs.txt> (accessed on 29 July 2019).
53. Lynch, R.S.; Swiggum, J.K.; Kondratiev, V.I.; Kaplan, D.L.; Stovall, K.; Fonseca, E.; Roberts, M.S.E.; Levin, L.; DeCesar, M.E.; Cui, B.; et al. The Green Bank North Celestial Cap Pulsar Survey. III. 45 New Pulsar Timing Solutions. *Astrophys. J.* **2018**, *859*, 93. [[CrossRef](#)]
54. Crawford, F.; Lyne, A.G.; Stairs, I.H.; Kaplan, D.L.; McLaughlin, M.A.; Freire, P.C.C.; Burgay, M.; Camilo, F.; D’Amico, N.; Faulkner, A.; et al. PSR J1723-2837: An Eclipsing Binary Radio Millisecond Pulsar. *Astrophys. J.* **2013**, *776*, 20. [[CrossRef](#)]
55. Kong, A.K.H.; Hui, C.Y.; Takata, J.; Li, K.L.; Tam, P.H.T. A NuSTAR Observation of the Gamma-Ray Emitting Millisecond Pulsar PSR J1723-2837. *Astrophys. J.* **2017**, *839*, 130. [[CrossRef](#)]
56. Barr, E.D.; Guillemot, L.; Champion, D.J.; Kramer, M.; Eatough, R.P.; Lee, K.J.; Verbiest, J.P.W.; Bassa, C.G.; Camilo, F.; Çelik, Ö.; et al. Pulsar searches of Fermi unassociated sources with the Effelsberg telescope. *Mon. Not. R. Astron. Soc.* **2013**, *429*, 1633–1642. [[CrossRef](#)]
57. Stovall, K.; Lynch, R.S.; Ransom, S.M.; Archibald, A.M.; Banaszak, S.; Biwer, C.M.; Boyles, J.; Dartez, L.P.; Day, D.; Ford, A.J.; et al. The Green Bank Northern Celestial Cap Pulsar Survey. I. Survey Description, Data Analysis, and Initial Results. *Astrophys. J.* **2014**, *791*, 67. [[CrossRef](#)]
58. Kaplan, D.L.; Stovall, K.; Ransom, S.M.; Roberts, M.S.E.; Kotulla, R.; Archibald, A.M.; Biwer, C.M.; Boyles, J.; Dartez, L.; Day, D.F.; et al. Discovery of the Optical/Ultraviolet/Gamma-Ray Counterpart to the Eclipsing Millisecond Pulsar J1816+4510. *Astrophys. J.* **2012**, *753*, 174. [[CrossRef](#)]
59. Parent, E.; Kaspi, V.M.; Ransom, S.M.; Freire, P.C.C.; Brazier, A.; Camilo, F.; Chatterjee, S.; Cordes, J.M.; Crawford, F.; Deneva, J.S.; et al. Eight Millisecond Pulsars Discovered in the Arecibo PALFA Survey. *Astrophys. J.* **2019**, *886*, 148. [[CrossRef](#)]
60. Stovall, K.; Allen, B.; Bogdanov, S.; Brazier, A.; Camilo, F.; Cardoso, F.; Chatterjee, S.; Cordes, J.M.; Crawford, F.; Deneva, J.S.; et al. Timing of Five PALFA-discovered Millisecond Pulsars. *Astrophys. J.* **2016**, *833*, 192. [[CrossRef](#)]
61. Fruchter, A.S.; Stinebring, D.R.; Taylor, J.H. A millisecond pulsar in an eclipsing binary. *Nature* **1988**, *333*, 237–239. [[CrossRef](#)]
62. Reynolds, M.T.; Callanan, P.J.; Fruchter, A.S.; Torres, M.A.P.; Beer, M.E.; Gibbons, R.A. The light curve of the companion to PSR B1957+20. *Mon. Not. R. Astron. Soc.* **2007**, *379*, 1117–1122. [[CrossRef](#)]
63. Huang, R.H.H.; Kong, A.K.H.; Takata, J.; Hui, C.Y.; Lin, L.C.C.; Cheng, K.S. X-ray Studies of the Black Widow Pulsar PSR B1957+20. *Astrophys. J.* **2012**, *760*, 92. [[CrossRef](#)]
64. Wu, E.M.H.; Takata, J.; Cheng, K.S.; Huang, R.H.H.; Hui, C.Y.; Kong, A.K.H.; Tam, P.H.T.; Wu, J.H.K. Orbital-phase-dependent Gamma-Ray Emissions from the Black Widow Pulsar. *Astrophys. J.* **2012**, *761*, 181. [[CrossRef](#)]
65. Shaifullah, G.; Verbiest, J.P.W.; Freire, P.C.C.; Tauris, T.M.; Wex, N.; Osłowski, S.; Stappers, B.W.; Bassa, C.G.; Caballero, R.N.; Champion, D.J.; et al. 21 year timing of the black-widow pulsar J2051-0827. *Mon. Not. R. Astron. Soc.* **2016**, *462*, 1029–1038. [[CrossRef](#)]

66. Stappers, B.W.; van Kerkwijk, M.H.; Lane, B.; Kulkarni, S.R. The Light Curve of the Companion to PSR J2051-0827. *Astrophys. J. Lett.* **1999**, *510*, L45–L48. [[CrossRef](#)]
67. Guillemot, L.; Octau, F.; Cognard, I.; Desvignes, G.; Freire, P.C.C.; Smith, D.A.; Theureau, G.; Burnett, T.H. Timing of PSR J2055+3829, an eclipsing black widow pulsar discovered with the Nançay Radio Telescope. *arXiv* **2019**, arXiv:1907.09778.
68. Bellm, E.C.; Kaplan, D.L.; Breton, R.P.; Phinney, E.S.; Bhallerao, V.B.; Camilo, F.; Dahal, S.; Djorgovski, S.G.; Drake, A.J.; Hessels, J.W.T.; et al. Properties and Evolution of the Redback Millisecond Pulsar Binary PSR J2129-0429. *Astrophys. J.* **2016**, *816*, 74. [[CrossRef](#)]
69. Kong, A.K.H.; Takata, J.; Hui, C.Y.; Zhao, J.; Li, K.L.; Tam, P.H.T. Broad-band high-energy emissions of the redback millisecond pulsar PSR J2129-0429. *Mon. Not. R. Astron. Soc.* **2018**, *478*, 3987–3993. [[CrossRef](#)]
70. Schroeder, J.; Halpern, J. Observations and Modeling of the Companions of Short Period Binary Millisecond Pulsars: Evidence for High-mass Neutron Stars. *Astrophys. J.* **2014**, *793*, 78. [[CrossRef](#)]
71. Keith, M.J.; Johnston, S.; Ray, P.S.; Ferrara, E.C.; Saz Parkinson, P.M.; Çelik, Ö.; Belfiore, A.; Donato, D.; Cheung, C.C.; Abdo, A.A.; et al. Discovery of millisecond pulsars in radio searches of southern Fermi Large Area Telescope sources. *Mon. Not. R. Astron. Soc.* **2011**, *414*, 1292–1300. [[CrossRef](#)]
72. An, H.; Romani, R.W.; Kerr, M. Signatures of Intra-binary Shock Emission in the Black Widow Pulsar Binary PSR J2241-5236. *Astrophys. J. Lett.* **2018**, *868*, L8. [[CrossRef](#)]
73. Pletsch, H.J.; Clark, C.J. Gamma-Ray Timing of Redback PSR J2339-0533: Hints for Gravitational Quadrupole Moment Changes. *Astrophys. J.* **2015**, *807*, 18. [[CrossRef](#)]
74. Camilo, F.; Lorimer, D.R.; Freire, P.; Lyne, A.G.; Manchester, R.N. Observations of 20 Millisecond Pulsars in 47 Tucanae at 20 Centimeters. *Astrophys. J.* **2000**, *535*, 975–990. [[CrossRef](#)]
75. Becker, W.; Huang, H.H.; Prinz, T. X-ray Counterparts of Millisecond Pulsars in Globular Clusters. *arXiv* **2010**, arXiv:1006.0335.
76. Cadelano, M.; Pallanca, C.; Ferraro, F.R.; Salaris, M.; Dalessandro, E.; Lanzoni, B.; Freire, P.C.C. Optical Identification of He White Dwarfs Orbiting Four Millisecond Pulsars in the Globular Cluster 47 Tucanae. *Astrophys. J.* **2015**, *812*, 63. [[CrossRef](#)]
77. Bogdanov, S.; Grindlay, J.E.; van den Berg, M. An X-ray Variable Millisecond Pulsar in the Globular Cluster 47 Tucanae: Closing the Link to Low-Mass X-ray Binaries. *Astrophys. J.* **2005**, *630*, 1029–1036. [[CrossRef](#)]
78. Pallanca, C.; Ransom, S.M.; Ferraro, F.R.; Dalessandro, E.; Lanzoni, B.; Hessels, J.W.T.; Stairs, I.; Freire, P.C.C. Radio Timing and Optical Photometry of the Black Widow System PSR J1518+0204C in the Globular Cluster M5. *Astrophys. J.* **2014**, *795*, 29. [[CrossRef](#)]
79. Hessels, J.W.T.; Ransom, S.M.; Stairs, I.H.; Kaspi, V.M.; Freire, P.C.C. A 1.4 GHz Arecibo Survey for Pulsars in Globular Clusters. *Astrophys. J.* **2007**, *670*, 363–378. [[CrossRef](#)]
80. Lynch, R.S.; Freire, P.C.C.; Ransom, S.M.; Jacoby, B.A. The Timing of Nine Globular Cluster Pulsars. *Astrophys. J.* **2012**, *745*, 109. [[CrossRef](#)]
81. Coccozza, G.; Ferraro, F.R.; Possenti, A.; Beccari, G.; Lanzoni, B.; Ransom, S.; Rood, R.T.; D’Amico, N. A Puzzling Millisecond Pulsar Companion in NGC 6266. *Astrophys. J. Lett.* **2008**, *679*, L105. [[CrossRef](#)]
82. D’Amico, N.; Possenti, A.; Manchester, R.N.; Sarkissian, J.; Lyne, A.G.; Camilo, F. An Eclipsing Millisecond Pulsar with a Possible Main-Sequence Companion in NGC 6397. *Astrophys. J. Lett.* **2001**, *561*, L89–L92. [[CrossRef](#)]
83. Kaluzny, J.; Rucinski, S.M.; Thompson, I.B. Photometry and Spectroscopy of the Optical Companion to the Pulsar PSR J1740-5340 in the Globular Cluster NGC 6397. *Astron. J.* **2003**, *125*, 1546–1553. [[CrossRef](#)]
84. Freire, P.C.C.; Ransom, S.M.; Bégin, S.; Stairs, I.H.; Hessels, J.W.T.; Frey, L.H.; Camilo, F. Eight New Millisecond Pulsars in NGC 6440 and NGC 6441. *Astrophys. J.* **2008**, *675*, 670–682. [[CrossRef](#)]
85. Hobbs, G.; Faulkner, A.; Stairs, I.H.; Camilo, F.; Manchester, R.N.; Lyne, A.G.; Kramer, M.; D’Amico, N.; Kaspi, V.M.; Possenti, A.; et al. The Parkes multibeam pulsar survey—IV. Discovery of 180 pulsars and parameters for 281 previously known pulsars. *Mon. Not. R. Astron. Soc.* **2004**, *352*, 1439–1472. [[CrossRef](#)]
86. Ransom, S.M.; Hessels, J.W.T.; Stairs, I.H.; Freire, P.C.C.; Camilo, F.; Kaspi, V.M.; Kaplan, D.L. Twenty-One Millisecond Pulsars in Terzan 5 Using the Green Bank Telescope. *Science* **2005**, *307*, 892–896. [[CrossRef](#)] [[PubMed](#)]
87. Hessels, J.W.T.; Ransom, S.M.; Stairs, I.H.; Freire, P.C.C.; Kaspi, V.M.; Camilo, F. A Radio Pulsar Spinning at 716 Hz. *Science* **2006**, *311*, 1901–1904. [[CrossRef](#)] [[PubMed](#)]

88. Bogdanov, S.; van den Berg, M.; Servillat, M.; Heinke, C.O.; Grindlay, J.E.; Stairs, I.H.; Ransom, S.M.; Freire, P.C.C.; Bégin, S.; Becker, W. Chandra X-ray Observations of 12 Millisecond Pulsars in the Globular Cluster M28. *Astrophys. J.* **2011**, *730*, 81. [[CrossRef](#)]
89. Pallanca, C.; Dalessandro, E.; Ferraro, F.R.; Lanzoni, B.; Rood, R.T.; Possenti, A.; D'Amico, N.; Freire, P.C.; Stairs, I.; Ransom, S.M.; et al. The Optical Companion to the Binary Millisecond Pulsar J1824-2452H in the Globular Cluster M28. *Astrophys. J.* **2010**, *725*, 1165–1169. [[CrossRef](#)]
90. Pallanca, C.; Dalessandro, E.; Ferraro, F.R.; Lanzoni, B.; Beccari, G. The Optical Counterpart to the X-ray Transient IGR J1824-24525 in the Globular Cluster M28. *Astrophys. J.* **2013**, *773*, 122. [[CrossRef](#)]
91. Papitto, A.; Ferrigno, C.; Bozzo, E.; Rea, N.; Pavan, L.; Burderi, L.; Burgay, M.; Campana, S.; di Salvo, T.; Falanga, M.; et al. Swings between rotation and accretion power in a binary millisecond pulsar. *Nature* **2013**, *501*, 517. [[CrossRef](#)]
92. Lynch, R.S.; Ransom, S.M.; Freire, P.C.C.; Stairs, I.H. Six New Recycled Globular Cluster Pulsars Discovered with the Green Bank Telescope. *Astrophys. J.* **2011**, *734*, 89. [[CrossRef](#)]
93. Freire, P.C.C.; Hessels, J.W.T.; Nice, D.J.; Ransom, S.M.; Lorimer, D.R.; Stairs, I.H. The Millisecond Pulsars in NGC 6760. *Astrophys. J.* **2005**, *621*, 959–965. [[CrossRef](#)]
94. Cadelano, M.; Pallanca, C.; Ferraro, F.R.; Stairs, I.; Ransom, S.M.; Dalessandro, E.; Lanzoni, B.; Hessels, J.W.T.; Freire, P.C.C. Radio Timing and Optical Photometry of the Black Widow System PSR J1953+1846A in the Globular Cluster M71. *Astrophys. J.* **2015**, *807*, 91. [[CrossRef](#)]
95. Ransom, S.M.; Stairs, I.H.; Backer, D.C.; Greenhill, L.J.; Bassa, C.G.; Hessels, J.W.T.; Kaspi, V.M. Green Bank Telescope Discovery of Two Binary Millisecond Pulsars in the Globular Cluster M30. *Astrophys. J.* **2004**, *604*, 328–338. [[CrossRef](#)]
96. Hui, C.Y. Spider Invasion Across the Galaxy. *J. Astron. Space Sci.* **2014**, *31*, 101–120. [[CrossRef](#)]
97. van den Heuvel, E.P.J.; van Paradijs, J. Fate of the companion stars of ultra-rapid pulsars. *Nature* **1988**, *334*, 227–228. [[CrossRef](#)]
98. Kluzniak, W.; Ruderman, M.; Shaham, J.; Tavani, M. Nature and evolution of the eclipsing millisecond binary pulsar PSR1957+20. *Nature* **1988**, *334*, 225–227. [[CrossRef](#)]
99. Ruderman, M.; Shaham, J.; Tavani, M. Accretion turnoff and rapid evaporation of very light secondaries in low-mass X-ray binaries. *Astrophys. J.* **1989**, *336*, 507–518. [[CrossRef](#)]
100. Ruderman, M.; Shaham, J.; Tavani, M.; Eichler, D. Late evolution of very low mass X-ray binaries sustained by radiation from their primaries. *Astrophys. J.* **1989**, *343*, 292–312. [[CrossRef](#)]
101. Stappers, B.W.; Gaensler, B.M.; Kaspi, V.M.; van der Klis, M.; Lewin, W.H.G. An X-ray Nebula Associated with the Millisecond Pulsar B1957+20. *Science* **2003**, *299*, 1372–1374. [[CrossRef](#)]
102. Cheng, K.S.; Taam, R.E.; Wang, W. Pulsar Wind Nebulae and the Non-thermal X-ray Emission of Millisecond Pulsars. *Astrophys. J.* **2006**, *641*, 427–437. [[CrossRef](#)]
103. Kargaltsev, O.; Rangelov, B.; Pavlov, G.G. Gamma-ray and X-ray Properties of Pulsar Wind Nebulae and Unidentified Galactic TeV Sources. In *The Universe Evolution. Astrophysical and Nuclear Aspects*; Nova Science Publishers, Inc.: New York, NY, USA, 2013
104. Hui, C.Y.; Becker, W. Searches for diffuse X-ray emission around millisecond pulsars: An X-ray nebula associated with PSR J2124-3358. *Astron. Astrophys.* **2006**, *448*, L13–L17. [[CrossRef](#)]
105. Lee, J.; Hui, C.Y.; Takata, J.; Lin, L.C.C. Discovery of an X-ray nebula in the field of millisecond pulsar PSRJ1911–1114. *Astron. Astrophys.* **2018**, *620*, L14. [[CrossRef](#)]
106. Homer, L.; Szkody, P.; Chen, B.; Henden, A.; Schmidt, G.; Anderson, S.F.; Silvestri, N.M.; Brinkmann, J. XMM-Newton and Optical Follow-up Observations of SDSS J093249.57+472523.0 and SDSS J102347.67+003841.2. *Astron. J.* **2006**, *131*, 562–570. [[CrossRef](#)]
107. Wang, Z.; Archibald, A.M.; Thorstensen, J.R.; Kaspi, V.M.; Lorimer, D.R.; Stairs, I.; Ransom, S.M. SDSS J102347.6+003841: A Millisecond Radio Pulsar Binary That Had a Hot Disk During 2000-2001. *Astrophys. J.* **2009**, *703*, 2017–2023. [[CrossRef](#)]
108. Tam, P.H.T.; Hui, C.Y.; Huang, R.H.H.; Kong, A.K.H.; Takata, J.; Lin, L.C.C.; Yang, Y.J.; Cheng, K.S.; Taam, R.E. Evidence for gamma-ray emission from the low-mass x-ray binary system first J102347.6+003841. *Astrophys. J. Lett.* **2010**, *724*, L207–L211. [[CrossRef](#)]
109. Stappers, B.W.; Archibald, A.; Bassa, C.; Hessels, J.; Janssen, G.; Kaspi, V.; Lyne, A.; Patruno, A.; Hill, A.B. State-change in the “transition” binary millisecond pulsar J1023+0038. *Astron. Telegr.* **2013**, 5513.

110. Patruno, A.; Archibald, A.M.; Hessels, J.W.T.; Bogdanov, S.; Stappers, B.W.; Bassa, C.G.; Janssen, G.H.; Kaspi, V.M.; Tendulkar, S.; Lyne, A.G. A New Accretion Disk around the Missing Link Binary System PSR J1023+0038. *Astrophys. J.* **2014**, *781*, L3. [[CrossRef](#)]
111. Halpern, J.P.; Gaidos, E.; Sheffield, A.; Price-Whelan, A.M.; Bogdanov, S. Optical Observations of the Binary MSP J1023+0038 in a New Accreting State. *Astron. Telegr.* **2013**, *5514*, 1.
112. Bogdanov, S.; Archibald, A.M.; Hessels, J.W.T.; Kaspi, V.M.; Lorimer, D.; McLaughlin, M.A.; Ransom, S.M.; Stairs, I.H. A Chandra X-ray Observation of the Binary Millisecond Pulsar PSR J1023+0038. *Astrophys. J.* **2011**, *742*, 97. [[CrossRef](#)]
113. de Martino, D.; Falanga, M.; Bonnet-Bidaud, J.-M.; Belloni, T.; Mouchet, M.; Masetti, N.; Andruchow, I.; Cellone, S.A.; Mukai, K.; Matt, G. The intriguing nature of the high-energy gamma ray source XSS J12270-4859. *Astron. Astrophys.* **2010**, *515*, 25. [[CrossRef](#)]
114. Bassa, C.G.; Patruno, A.; Hessels, J.W.T.; Archibald, A.M.; Mahony, E.K.; Monard, B.; Keane, E.F.; Bogdanov, S.; Stappers, B.W.; Janssen, G.H.; et al. A possible state transition in the low-mass X-ray binary XSS J12270-4859. *Astron. Telegr.* **2013**, *5647*.
115. Tam, P.; Kong, A.; Li, K. Fermi/LAT and Swift/XRT observations of XSS J12270-4859/2FGL J1227.7-4853. *Astron. Telegr.* **2013**, *5652*.
116. Roy, J.; Bhattacharyya, B.; Ray, P. GMRT discovery of a 1.69 ms radio pulsar associated with XSS J12270-4859. *Astron. Telegr.* **2014**, *5890*.
117. Hui, C.Y.; Hu, C.P.; Park, S.M.; Takata, J.; Li, K.L.; Tam, P.H.T.; Lin, L.C.C.; Kong, A.K.H.; Cheng, K.S.; Kim, C. Exploring the Intrabinary Shock from the Redback Millisecond Pulsar PSR J2129-0429. *Astrophys. J.* **2015**, *801*, L27. [[CrossRef](#)]
118. Possenti, A.; Cerutti, R.; Colpi, M.; Mereghetti, S. Re-examining the X-ray versus spin-down luminosity correlation of rotation powered pulsars. *Astron. Astrophys.* **2002**, *387*, 993. [[CrossRef](#)]
119. Hui, C.Y.; Cheng, K.S.; Taam, R.E. Dynamical Formation of Millisecond Pulsars in Globular Clusters. *Astrophys. J.* **2010**, *714*, 1149–1154. [[CrossRef](#)]
120. Saz Parkinson, P.M.; Xu, H.; Yu, P.L.H.; Salvetti, D.; Marelli, M.; Falcone, A.D. Classification and ranking of Fermi LAT gamma-ray sources from the 3FGL catalog using machine learning techniques. *Astrophys. J.* **2016**, *820*, 8. [[CrossRef](#)]
121. Leung, A.P.; Tong, Y.; Li, R.; Luo, S.; Hui, C.Y. A Novel Framework for Gamma-ray Source Classification using Automatic Feature Selection. *Proc. Sci.* **2017**, *312*, 133.
122. Li, K.-L.; Kong, A.K.H.; Hou, X.; Mao, J.; Strader, J.; Chomiuk, L.; Tremou, E. Discovery of a Redback Millisecond Pulsar Candidate: 3FGL J0212.1+5320. *Astrophys. J.* **2016**, *833*, 143. [[CrossRef](#)]
123. Linares, M.; Miles-Páez, P.; Rodríguez-Gil, P.; Shahbaz, T.; Casares, J.; Fariña, C.; Karjalainen, R. A millisecond pulsar candidate in a 21-h orbit: 3FGL J0212.1+5320. *Mon. Not. R. Astron. Soc.* **2017**, *465*, 4602. [[CrossRef](#)]
124. Strader, J.; Li, K.-L.; Chomiuk, L.; Heinke, C.O.; Udalski, A.; Peacock, M.; Shishkovsky, L.; Tremou, E. A New gamma-Ray Loud Eclipsing Low-mass X-ray Binary. *Astrophys. J.* **2016**, *831*, 89. [[CrossRef](#)]
125. Strader, J.; Chomiuk, L.; Sonbas, E.; Sokolovsky, K.; Sand, D.J.; Moskvitin, A.S.; Cheung, C.C. 1FGL J0523.5-2529: A New Probable Gamma-Ray Pulsar Binary. *Astrophys. J.* **2014**, *788*, L27. [[CrossRef](#)]
126. Xing, Y.; Wang, Z.; Ng, C.Y. Fermi Variability Study of the Candidate Pulsar Binary 2FGL J0523.3-2530. *Astrophys. J.* **2014**, *795*, 88. [[CrossRef](#)]
127. Salvetti, D.; Mignani, R.P.; De Luca, A.; Marelli, M.; Pallanca, C.; Breeveld, A.A.; Hüsemann, P.; Belfiore, A.; Becker, W.; Greiner, J. A multiwavelength investigation of candidate millisecond pulsars in unassociated gamma-ray sources. *Mon. Not. R. Astron. Soc.* **2017**, *470*, 466 [[CrossRef](#)]
128. Halpern, J.P.; Strader, J.; Li, M. A Likely Redback Millisecond Pulsar Counterpart of 3FGL J0838.8-2829. *Astrophys. J.* **2017**, *844*, 150. [[CrossRef](#)]
129. Swihart, S.J.; Strader, J.; Johnson, T.J.; Cheung, C.C.; Sand, D.; Chomiuk, L.; Wasserman, A.; Larsen, S.; Brodie, J.P.; Simonian, G.V.; et al. 2FGL J0846.0+2820: A New Neutron Star Binary with a Giant Secondary and Variable  $\gamma$ -Ray Emission. *Astrophys. J.* **2017**, *851*, 31. [[CrossRef](#)]
130. Li, K.-L.; Hou, X.; Strader, J.; Takata, J.; Kong, A.K.H.; Chomiuk, L.; Swihart, S.J.; Hui, C.Y.; Cheng, K.S. Multiwavelength Observations of a New Redback Millisecond Pulsar Candidate: 3FGL J0954.8-3948. *Astrophys. J.* **2018**, *863*, 194. [[CrossRef](#)]

131. Coti Zelati, F.; Papitto, A.; de Martino, D.; Buckley, D.A.H.; Odendaal, A.; Li, J.; Russell, T.D.; Torres, D.F.; Mazzola, S.M.; Bozzo, E.; et al. Prolonged sub-luminous state of the new transitional pulsar candidate CXOU J110926.4-650224. *Astron. Astrophys.* **2019**, *622*, A211. [[CrossRef](#)]
132. Bogdanov, S.; Halpern, J.P. Identification of the High-energy Gamma-Ray Source 3FGL J1544.6-1125 as a Transitional Millisecond Pulsar Binary in an Accreting State. *Astrophys. J.* **2015**, *803*, L27. [[CrossRef](#)]
133. Britt, C.T.; Strader, J.; Chomiuk, L.; Tremou, E.; Peacock, M.; Halpern, J.; Salinas, R. Orbital Dynamics of Candidate Transitional Millisecond Pulsar 3FGL J1544.6-1125: An Unusually Face-on System. *Astrophys. J.* **2017**, *849*, 21. [[CrossRef](#)]
134. Romani, R.W.; Filippenko, A.V.; Cenko, S.B. 2FGL J1653.6-0159: A New Low in Evaporating Pulsar Binary Period. *Astrophys. J.* **2014**, *793*, L20. [[CrossRef](#)]
135. Kong, A.K.H.; Jin, R.; Yen, T.-C.; Hu, C.-P.; Hui, C.Y.; Tam, P.H.T.; Takata, J.; Lin, L.C.C.; Cheng, K.S.; Park, S.M.; et al. Discovery of an Ultracompact Gamma-Ray Millisecond Pulsar Binary Candidate. *Astrophys. J.* **2014**, *794*, L22. [[CrossRef](#)]
136. Romani, R.W. A Likely Millisecond Pulsar Binary Counterpart for Fermi Source 2FGL J2039.6-5620. *Astrophys. J.* **2015**, *812*, L24. [[CrossRef](#)]
137. Salvetti, D.; Mignani, R.P.; De Luca, A.; Delvaux, C.; Pallanca, C.; Belfiore, A.; Marelli, M.; Breeveld, A.A.; Greiner, J.; Becker, W.; et al. Multi-wavelength Observations of 3FGL J2039.6-5618: A Candidate Redback Millisecond Pulsar. *Astrophys. J.* **2015**, *814*, 88. [[CrossRef](#)]
138. Ng, C.W.; Takata, J.; Strader, J.; Li, K.L.; Cheng, K.S. Evidence on the Orbital Modulated Gamma-Ray Emissions from the Redback Candidate 3FGL J2039.6-5618. *Astrophys. J.* **2018**, *867*, 90. [[CrossRef](#)]
139. Arons, J.; Tavani, M. High-energy emission from the eclipsing millisecond pulsar PSR 1957+20. *Astrophys. J.* **1993**, *403*, 249. [[CrossRef](#)]
140. Bednarek, W.; Sitarek, J. High-energy emission from the nebula around the Black Widow binary system containing millisecond pulsar B1957+20. *Astron. Astrophys.* **2013**, *550*, A39. [[CrossRef](#)]
141. Ahnen, M.L.; Ansoldi, S.; Antonelli, L.A.; Arcaro, C.; Babić, A.; Banerjee, B.; Bangale, P.; Barres de Almeida, U.; Barrio, J.A.; Becerra González, J.; et al. Observation of the black widow B1957+20 millisecond pulsar binary system with the MAGIC telescopes. *Mon. Not. R. Astron. Soc.* **2017**, *470*, 4608–4617. [[CrossRef](#)]



© 2019 by the authors. Licensee MDPI, Basel, Switzerland. This article is an open access article distributed under the terms and conditions of the Creative Commons Attribution (CC BY) license (<http://creativecommons.org/licenses/by/4.0/>).